SYNTHESES AND INVESTIGATION OF OPTOELECTRONIC PROPERTIES
OF BENZOTHIADIAZOLE AND BENZOTRIAZOLE CONTAINING
CONJUGATED POLYMERS

A THESIS SUBMITTED TO
THE GRADUATE SCHOOL OF NATURAL AND APPLIED SCIENCES
OF
MIDDLE EAST TECHNICAL UNIVERSITY

BY

DUYGU KELEŞ

IN PARTIAL FULFILLMENT OF THE REQUIREMENTS
FOR
THE DEGREE OF MASTER OF SCIENCE
IN
POLYMER SCIENCE AND TECHNOLOGY

AUGUST 2017

Approval of the thesis:

SYNTHESES AND INVESTIGATION OF OPTOELECTRONIC PROPERTIES OF BENZOTHIADIAZOLE AND BENZOTRIAZOLE CONTAINING CONJUGATED POLYMERS

Submitted by **DUYGU KELEŞ in** partial fulfillment of the requirements for the degree of **Master of Science in Polymer Science and Technology Department, Middle East Technical University** by,

Prof. Dr. Gülbin Dural Ünver   _____
Dean, Graduate School of **Natural and Applied Sciences**

Prof. Dr. Necati Özkan   _____
Head of Department, **Polymer Science and Technology**

Prof. Dr. Ali Çırpan   _____
Supervisor, **Department of Chemistry, METU**

Assoc. Prof. Dr. Yasemin Arslan Udum   _____
Co-supervisor, **Department of Advanced Technologies, Gazi University**

Examining Committee Members:

Prof. Dr. Levent Toppare   _____
Chemistry Dept., METU

Prof. Dr. Ali Çırpan   _____
Chemistry Dept., METU

Assoc. Prof. Dr. Yasemin Arslan Udum   _____
Advanced Technologies Dept., Gazi University

Assoc. Prof. Dr. Emren Nalbant Esentürk   _____
Chemistry Dept., METU

Asst. Prof. Dr. Görkem Günbaş   _____
Chemistry Dept., METU

Date: 14/08/2017

I hereby declare that all information in this document has been obtained and presented in accordance with academic rules and ethical conduct. I also declare that, as required by these rules and conduct, I have fully cited and referenced all material and results that are not original to this work.

Name, Last name: Duygu KELEŞ

Signature:

ABSTRACT

SYNTHESES AND INVESTIGATION OF OPTOELECTRONIC PROPERTIES OF BENZOTHIADIAZOLE AND BENZOTRIAZOLE CONTAINING CONJUGATED POLYMERS

Keleş, Duygu

M. Sc., Polymer Science and Technology Department
Supervisor: Prof. Dr. Ali Çırpan
Co-Supervisor: Assoc.Prof. Dr. Yasemin Arslan Udum
August 2017, 69 pages

Benzothiadiazole is one of the most widely used acceptor units in Donor–Acceptor copolymers for organic solar cells (OSCs) with its strong electron withdrawing ability. It is also known that fluorine atom substitution directly to the backbone of conjugated polymers can improve the important parameters such as power conversion efficiency (PCE), open-circuit voltage (V_{oc}), short-circuit current density (J_{sc}), and fill factor (FF) of OSCs. Besides benzothiadiazole, benzotriazole is another acceptor moiety which is used in OSCs frequently. In this study, two different random polymers, including benzothiadiazole and benzotriazole as the accepting units and benzodithiophene as the donor unit, were synthesized via Stille polymerization reaction. Moreover, effects of fluorine atom on optical, electrochemical and optoelectronic properties were investigated. Optical band gap values of **P1** and **P2** were found as 1.78 eV and 1.72 eV, respectively. After

characterization of polymers via UV-Vis-NIR spectroscopy, cyclic voltammetry (CV), gel permeation chromatography (GPC) and thermal analysis, the polymers were used to construct organic photovoltaic cells. Fabrication and characterization of them was performed in nitrogen-filled glove box system. While the polymers act as electron donor, $PC_{70}BM$ was electron acceptor in the OSCs which were constructed according to ITO/PEDOT:PSS/Polymer:$PC_{70}BM$/LiF/Al. Morphology of Polymer:$PC_{70}BM$ blends was investigated with Atomic Force Microscopy (AFM). In consequence of measurement under standard AM 1.5 G illumination (100 mW/cm^2), the highest power conversion efficiency was found as 4.13% for **P1** and 3.80% for **P2**.

Keywords: Benzotriazole, benzothiadiazole, conjugated polymers, fluorination, organic solar cell

ÖZ

BENZOTİYADİAZOL VE BENZOTRİYAZOL İÇEREN KONJUGE POLİMERLERİN SENTEZİ VE OPTOELEKTRONİK ÖZELLİKLERİNİN İNCELENMESİ

Keleş, Duygu

Yüksek Lisans, Polimer Bilimi ve Teknolojisi Bölümü

Tez Yöneticisi: Prof. Dr. Ali Çırpan

Ortak Tez Yöneticisi: Doç. Dr. Yasemin Arslan Udum

Ağustos 2017, 69 sayfa

Benzotiyadiazol, güçlü elektron geri çekme yeteneği ile organik güneş pilleri (OSC'ler) için Donör-Akseptör kopolimerlerinde kabul gören en yaygın birimlerden biridir. Ayrıca, flor atomlarının konjuge polimerlerin omurgasına direk olarak ikame edilebilmesi, güç dönüştürme verimliliği (PCE), açık devre gerilimi (V_{oc}), kısa devre akım yoğunluğu (J_{sc}) ve dolgu faktörü (FF) gibi önemli parametreleri artırabileceği bilinmektedir. Benzotiyadiazolun yanı sıra, benzotriazol, OSC'lerde sıklıkla kullanılan bir başka akseptör parçasıdır. Bu çalışmada, elektron çekici üniteleri olarak benzotiadiazol ve benzotriazol ve elektron verici ünite olarak da benzoditiyofen içeren iki farklı rastgele polimer Stille polimerizasyonu reaksiyonu ile sentezlenmiştir. Ayrıca flor atomunun optik, elektrokimyasal ve optoelektronik özelliklere etkileri araştırılmıştır. **P1** ve **P2**'nin optik bant aralık değerleri sırasıyla 1.72 eV ve 1.78 eV olarak bulundu. Polimerlerin UV-Vis-NIR spektroskopisi,

dönüşümlü voltametri (CV), jel geçirgenlik kromatografisi (GPC) ve termal analizden sonra, polimerler organik fotovoltaik hücreler oluşturmak için kullanıldı. Azotla doldurulmuş havasız ortam kabininde, bunların imalatı ve karakterizasyonu gerçekleştirildi. Polimerler elektron verici kısım olarak görev yaparken, ITO / PEDOT: PSS / Polimer: $PC_{70}BM$ / LiF / Al'e göre yapılandırılmış OSC'lerde $PC_{70}BM$, elektron alıcıdır. Polimerin:$PC_{70}BM$ harmanlarının morfolojisi, Atomik Kuvvet Mikroskopisi (AFM) ile araştırıldı. Standart AM 1,5 G aydınlatma (100 mW / cm^2) altında yapılan ölçüm sonucunda, en yüksek güç dönüşüm verimliliği, **P1** için% 4.13 ve **P2** için% 3.80 olarak bulundu.

Anahtar Kelimeler: Benzotriazol, benzotiadiazol, konjüge polimerler, flüorinasyon, organik güneş pilleri

ACKNOWLEDGEMENTS

TABLE OF CONTENTS

LIST OF TABLES

LIST OF FIGURES

LIST OF ABBREVIATIONS

ACN   Acetonitrile

AM   Air Mass

AFM   Atomic Force Microscopy

BDT   Benzodithiophene

BHJ   Bulk heterojunction

BT   Benzothiadiazole

BTz   Benzotriazole

CE   Counter Electrode

$CHCl_3$ Chloroform

CP   Conjugated Polymer

CV   Cyclic Voltammetry

D-A   Donor-Acceptor

DIO   Diiodooctane

DCM   Dichloromethane

DSC   Differential Scanning Calorimetry

ECD   Electrochromic Device

FF   Fill factor

GPC	Gel permeation chromatography
HOMO	Highest occupied molecular orbital
ITO	Indium-doped tin oxide
IPCE	Incident photon to current efficiency
J_{sc}	Short Circuit Current Density
LUMO	Lowest unoccupied molecular orbital
OFET	Organic Field Effect Transistor
OLED	Organic Light Emitting Diode
OSC	Organic Solar Cell
PCE	Power Conversion Efficiency
PCBM	[6,6]-Phenyl-C61-butyric acid methyl ester
PEDOT:PSS poly(styrenesulfonate)	Poly(3,4-ethylenedioxythiophene)-
RE	Reference Electrode
$TBAPF_6$	Tetrabutylammonium hexafluorophosphate
TGA	Thermogravimetry Analyses
TCO	Transparent Conductive Oxide
V_{oc}	Open Circuit Voltage
WE	Working Electrode

INTRODUCTION

1.1. World Energy Production

Increasing in human population brings a very critical problem; the energy consumption. Nowadays, dominant energy production source is fossil fuels. This fact was reported in World Energy Sources Report[1] in 2016 shown in Figure 1.
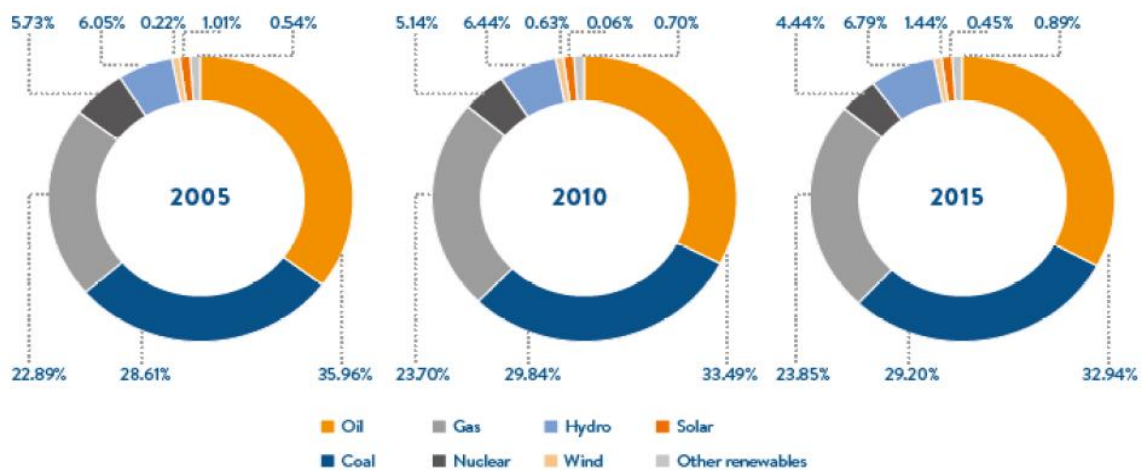
Figure 1. Energy Consumption over the Past 15 Years

Unfortunately, fossil fuels have been exhausted rapidly around the world. Also, they have many drawbacks. Since they are non-renewable, they are limited in quantities. Combustion of these organic materials generates carbon dioxide which cause to air pollution and climate problems. Although nuclear energy is the other major power source, it is not widespread because of security and health risk. Therefore, searching

for reliable, cheap and environmentally friendly energy sources becomes a hot topic for many researchers.

1.2. Renewable Energy Sources

As a result of upcoming energy shortage, mankind desires to develop renewable energy sources. Hydroelectric energy, solar energy, wind energy, and geothermal energy are examples of renewable energy sources. Figure 2 summarizes[2] growing rate in renewable energy sources in 2014. Growing in solar photovoltaics takes attention because of possible advantage of solar energy. Although there are limitations in wind, geothermal and hydroelectric energy according to geographic region, solar energy is available in almost everywhere on the earth. Moreover, it is reliable and free.
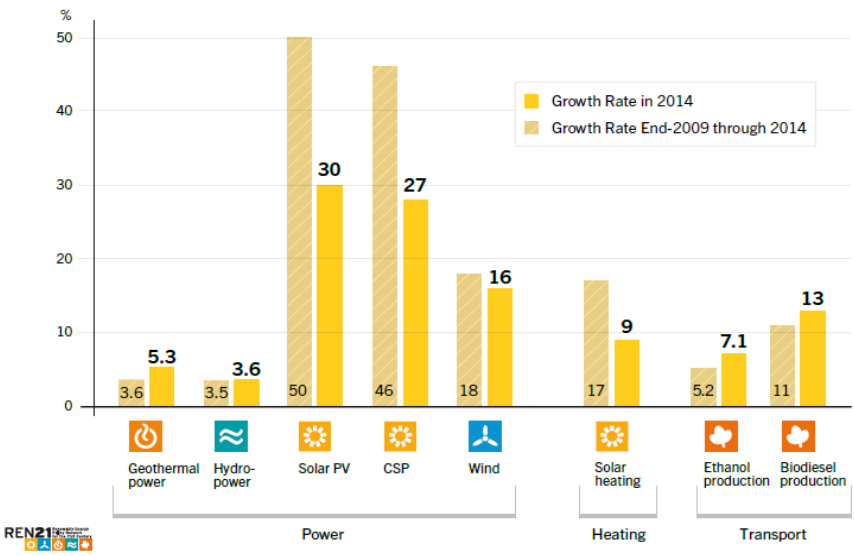
Figure 2. Growth Rates of Renewable Energy Capacity

1.3. Solar Cells

A device which converts solar energy into electrical energy called as solar cell. Today, predominant material in the solar cell market is silicon because of high abundance of it in the nature and high efficiency of its solar cells. Although silicon is

cheap material, low absorptivity of it requires thick absorbing layers, and high purities.[3] This makes silicon solar cells expensive. A cheaper alternative is organic solar cells (OSCs) with high absorption coefficients and low active layer thicknesses. However, although power conversion efficiency (PCE) of silicon solar cells has been reached to 26%,[4] organic solar cells shows lower PCE.

CHAPTER 2

ORGANIC SOLAR CELLS

Organic solar cells convert light into electrical energy and they are composed of carbon based semiconducting materials.[5] They are different from inorganic cells in terms of both working principle and production methods. Since they offer low cost manufacturing, they have become very popular for the two decades. Flexibility, solution processability, easy fabrication to large scale and low weight are the other advantages of OSCs with respect to inorganics.[6] On the other hand, low performance and instability problems are their main disadvantages.

2.1. Device Architectures of Organic Solar Cells

The simplest organic solar cells are based on single layer architecture. In this type, organic material is sandwiched between two electrodes and exciton dissociates only at the organic material-cathode interface which is shown in Figure 3. Electrostatic forces between two electrodes are insufficient for exciton dissociation. Therefore, single layer OSCs are suffer from poor fill factor and low efficiency.[7]
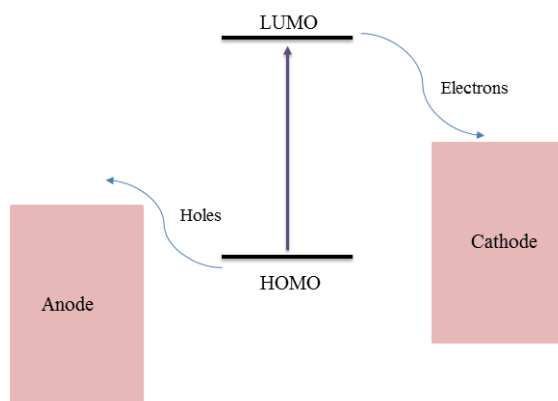
Figure 3. Single Layer Organic Solar Cells

In a bilayer OSC (Figure 4), electron acceptor layer is introduced between metal electrode and active material. Thus, device is consisting of p-type layer which provides hole transport and n-type layer which provides electron transport. Although they increase exciton diffusion possibility with respect to single layer, charge recombination is critical in bilayer OSC. For most OSC materials, exciton diffusion length is below 20 nm.[8] If layers are too thick, generated excitons may recombine before reach to electrodes. Losing of absorbed photons further away from the interface cause to low efficiency.[9]
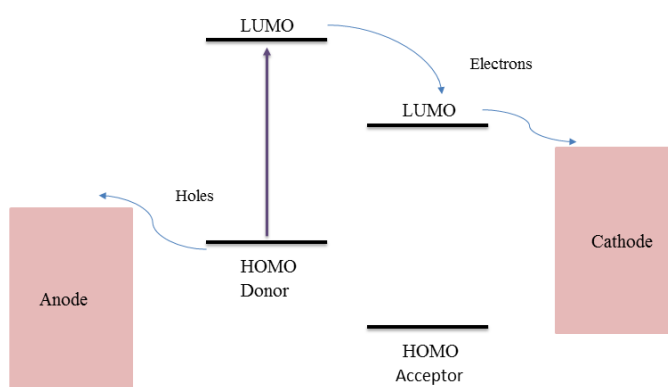
Figure 4. Bilayer Organic Solar Cells

With the discovery of bulk heterojunction (BHJ) structure, exciton diffusion problem could be solved and efficient charge transport can be provided. Because it is blend of

acceptor and donor phases, donor-acceptor length scale decrease to 10-20 nm, and interfacial area between of them increases.[10] Thus, efficiency of OSCs is improved. Structural differences between bilayer and bulk heterojunction is illustrated in Figure 5.
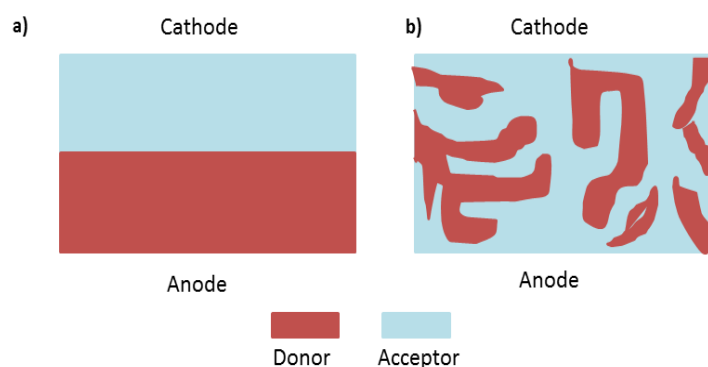
Figure 5. Active Layer of OSCs a) bilayer, b) bulk heterojunction

2.2. Device Fabrication of Organic Solar Cells

2.2.1. Substrate

Requirements of suitable substrate of OSCs are low cost, optical transparency, thermal, environmental and chemical stability. Glass is commonly used in OSCs as the substrate due to its low cost, stability, and transparency properties. Moreover, poly (ethylene terephthalate) (PET), poly (ether sulfonate) (PES), and polycarbonate can be preferred for providing flexibility.[11]

2.2.2. Anode

In OSCs, transparent conductive oxide (TCO) deposited on the substrate to provide conductivity. Indium-doped tin oxide (ITO) is commonly used as a TCO because it has both transparency and conductivity properties. The work function of ITO can be changed with surface treatment and cleaning. Surface treatments with oxidizing agents (e.g. oxygen plasma) results to increasing work function.[12] Increasing the

work function is desirable in OSCs because injection holes into the organic materials are provided with high work function electrodes.[13]

PEDOT:PSS (Poly(3,4-ethylenedioxythiophene)-poly(styrenesulfonate)) is commonly coated on ITO to provide matching with organic semiconductor layer. It serves as hole transport layer and also useful for planarization of ITO surface.[14]

2.2.3. Active Layer

Generally, active layer of BHJ OSCs consists of conjugated polymer and a small molecule like PCBM. After preparing solution of donor and acceptor components in a common solvent, it is coated on substrate. Performance of OSCs is affected from concentration of donor and acceptor in solution, solvent type, film thickness, additives and annealing.

2.2.4. Cathode

Applying a top metal contact to OSC is final step. The metal electrode is usually deposited via vacuum deposition. The metal is chosen based on work function, hence low work function metals are preferred for the good matching with LUMO of acceptor and effective electron collection.[10] However, low work function metal brings stability problems because stability is proportional to work function. Therefore, thin layer of LiF deposited between active layer and metal[15] and this approach increases OSC performance.[16]

Device fabrication of an OSC is shown in Figure 6.
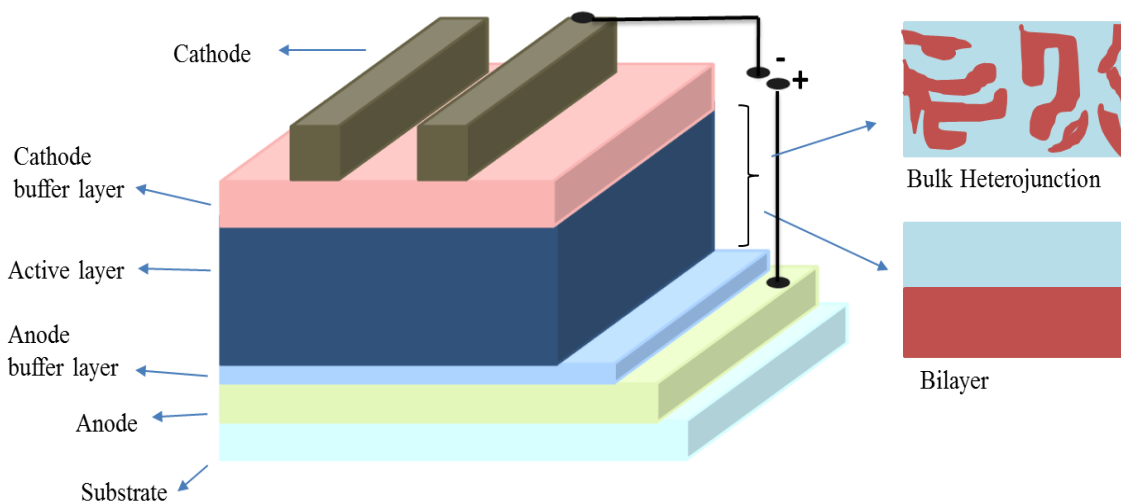
Figure 6. Layers of OSC

2.3. Working Principle of Organic Solar Cells

2.3.1. Light absorption and Exciton Formation

The primary circumstance of a substance to be useful in OSC is having a conjugated π electron system. In a conjugated system, valence electrons occupy at the π orbital, which is also known as the highest occupied molecular orbital (HOMO). When photon is absorbed, electron excites from the π (bonding) to the π^* (anti-bonding) orbital. These excitation generates electron-hole pairs called as exciton.[17]

2.3.2. Exciton Diffusion

Depending on the lifetime of excitons, they can diffuse through a shorter distance than 20 nm. Otherwise, they may recombine or separate to free electrons and holes.[18] Because of strong binding energy, exciton needs to move donor-acceptor interface to dissociate. At this interface, dissociation to hole and electron can be achieved by charge transfer.

9

2.3.3. Exciton Dissociation

This step covers splitting exciton to hole and electron in the donor-acceptor interlayer. Efficient splitting requires that exciton binding energy should be lower than energy differences between LUMO of donor and acceptor.[19]

2.3.4. Charge Transport

After generation of free charges owing to exciton dissociation, they are transported to and collected on electrodes. While holes move to the anode via donor compartment, electrons move to the cathode via acceptor compartment.

Figure 7 shows general working principle of OSCs.
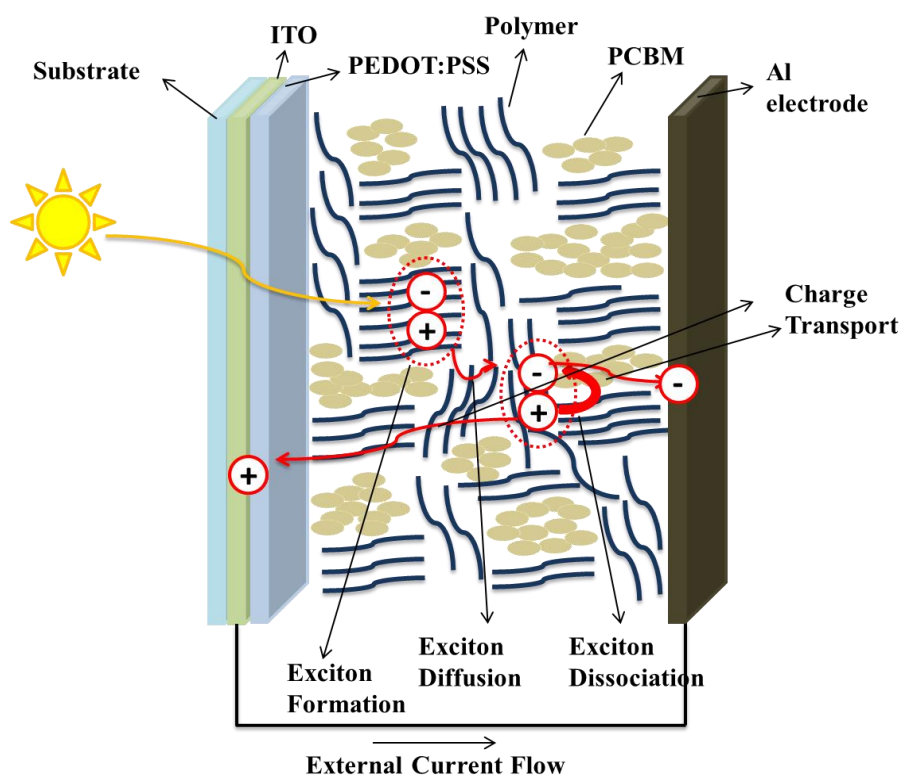
Figure 7. Working Principle of OSCs

2.4. Organic Solar Cell Parameters

While sunlight travels through the atmosphere, it may be reduced via absorption, reflection, or scattering. Air mass (AM) is measurement of sunlight that can reach the earth surface. It is calculated from the following equation;

$$AM = \frac{1}{\cos\theta}$$

where θ is the angle of incident sunlight to earth.

Path of sunlight through atmosphere changes during the day time (Figure 8). It is accepted that sunlight reach the earth with 48° angle and AM 1.5 G is used as the international AM.
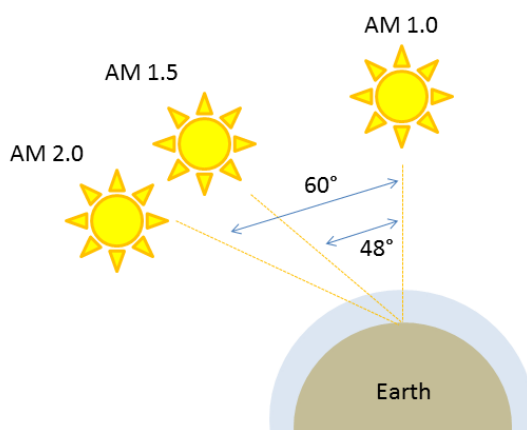
Figure 8. The solar radiation path through the earth's atmosphere in units of Air Mass

When a J-V curve (Figure 9) is obtained from the OSC measurement, the maximum power (P_{max}) can be calculated from the maximum value of the product of J and V.
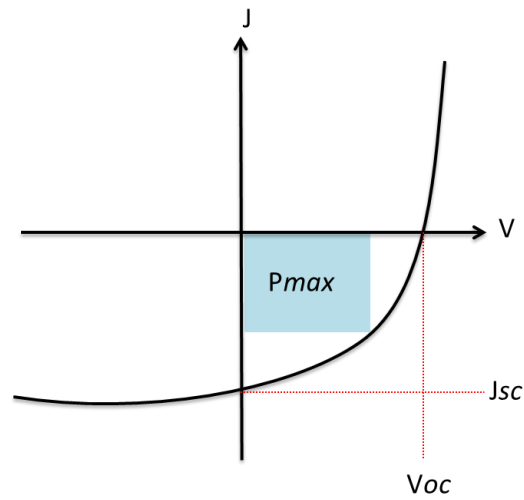
Figure 9. Typical J-V curve for an OSC

Fill factor (FF) is the ratio of maximum power generated by the OSC to product of V_{oc} and J_{sc}.

$$FF = \frac{Pmax}{VocxJsc}$$

Short Circuit Current Density (J_{sc}) is that how much current flow through the circuit when voltage is zero.

Open Circuit Voltage (V_{oc}) is amount of voltage when there is no current flow through the circuit.

Thus, Power Conversion Efficiency (η) is calculated from the following equation;

$$\eta = FF\frac{JscxVoc}{Pin}$$

CHAPTER 3

CONJUGATED POLYMERS FOR ORGANIC SOLAR CELLS

Conjugated polymers (CPs) are organic substances that contain alternating double bonds in backbone chain. In the recent years, they attracted attention because they combine plastic and semiconducting properties such as suitable band gap for electrical conductivity, flexibility, solution processability.[20] Thanks to these properties, CPs are used in organic solar cell (OSC), organic light emitting diode (OLED), electrochromic device (ECD), and organic field effect transistor (OFET) applications.[21]

3.1. Criteria for an Efficient Organic Solar Cells

3.1.1. Large Absorption

Solar energy consists of ultraviolet, visible and near-infrared regions. Figure 10 shows the solar irradiation spectrum at sea level.[22] To get maximum of solar energy, large absorption is required. Because PCBM derivatives, which are generally acceptor part of BHJ OSCs, have not sufficient absorption in higher than 400 nm,[23] the CP has become responsible for the large absorption. Thickness and the absorption coefficient of the photoactive layer are the factors which effect absorption in OSCs.
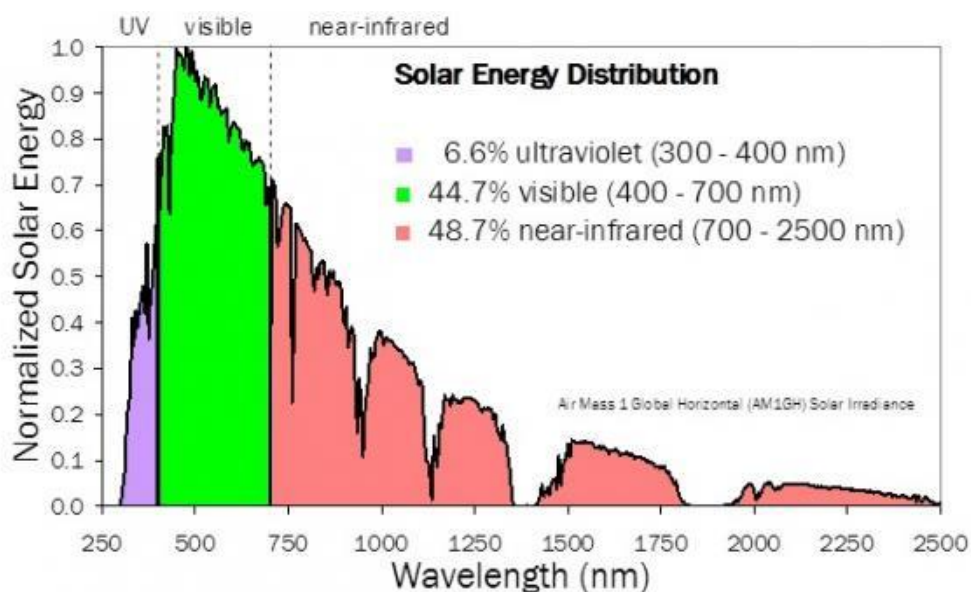
Figure 10. Solar Energy Distribution

3.1.2. Low Band Gap

The energy difference between HOMO and LUMO energy levels is called band gap. This description divides materials into three categories as insulators, conductors, and semiconductors. While insulators exhibit very large difference between these levels, there is no gap in conductors. On the other hand, the band gap of semiconductors is in the range of 1.5 and 3.0 eV.[24] Because of the maximum photon flux around 1.8 eV in solar emission, usage of low band gap polymers (Eg ≤1.8 eV) plays important role for the number of absorbed photons in OSCs.[25]

Donor-acceptor approach is the common way to adjust the band gap of the CPs. Two different units which are donor (electron rich) and acceptor (electron deficient) are involved on the same polymer backbone. The result of hybridization between HOMO level of the donor and LUMO level of the acceptor narrow band gap is obtained.[26] Also, resonance between donor and acceptor units increase electron delocalization and make electron transfer easier. Schematic view of donor- acceptor theory is given in Figure 11.
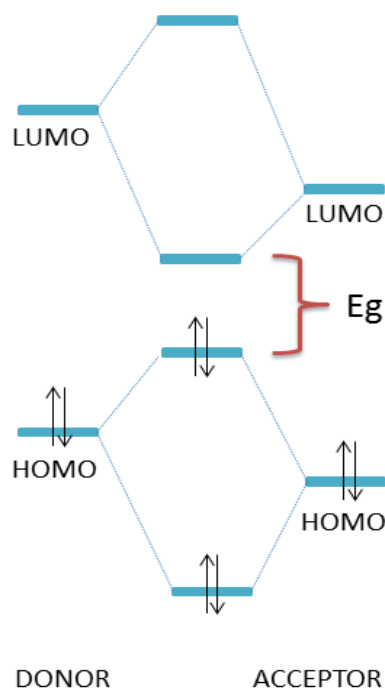
Figure 11. Orbital interaction of donor and acceptor component in DA approach

3.1.3. Morphology

Morphology in blend structure of photovoltaic cell can enhance charge transport ability and so PCE. Homogenous active layer, decreasing domain size, increasing domain purity and crystallization is favorable for charge transport. Solvent selection, use of chemical additives, changing of donor-acceptor blend ratio, and thermal annealing may affect active layer morphology.[27] X-ray scattering, Transmission Electron Microscopy (TEM), and Atomic Force Microscopy (AFM) are the common techniques used to investigate morphology.[28]

3.1.4. Suitable HOMO/LUMO energy level

Beside morphology, efficient charge transport also depends on HOMO and LUMO energy levels. To ensure stability, HOMO level of the polymer should be lower than air oxidation threshold (-5.2 eV).[29] In addition, deeper HOMO level causes an increase in V_{oc} and this contributes to high efficiency. To make electron transfer

from the donor polymer to acceptor polymer (usually PCBM), LUMO level of the donor polymer should be higher from the LUMO level of the acceptor polymer.

3.1.5. Solubility

Application of a polymer to OSC requires reasonable solubility. Commonly, alkyl chains are attached to a polymer chain to ensure solubility. While these chains do not affect absorption range or charge transport, they may affect structural organization and morphology in blend.

3.1.6. Stability

Durability and shelf time of OSC device determine commercialization of it. Degradation of active layer and oxidation of low work function electrode by air[30] are important problems for stability. In this manner, encapsulation and using stable electrodes can increase the stability of OSC devices.

3.2. Conduction in Conjugated Polymers

Although the most of polymers are insulators or semiconductors, conductivity of them can be increased with doping process which is defined as removal of an electron from the polymer backbone (p-doping) or injection of an electron to the polymer backbone (n-doping). This process can be achieved chemically (oxidized or reduced agents) or electrochemically. Because anions are very sensitive to oxygen, n-doping is not common for conjugated polymers. Types of doping process are depicted in Figure 12.
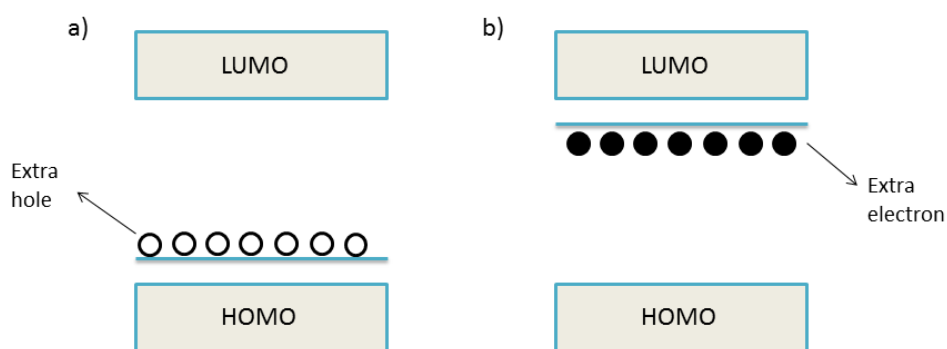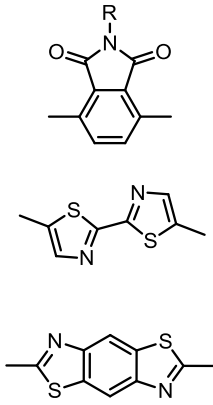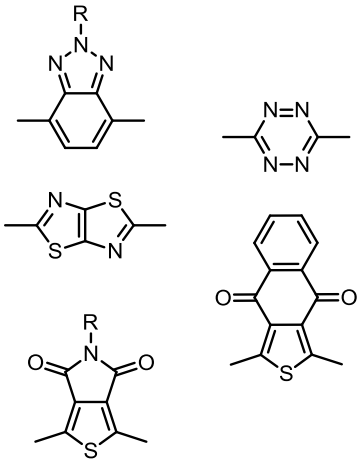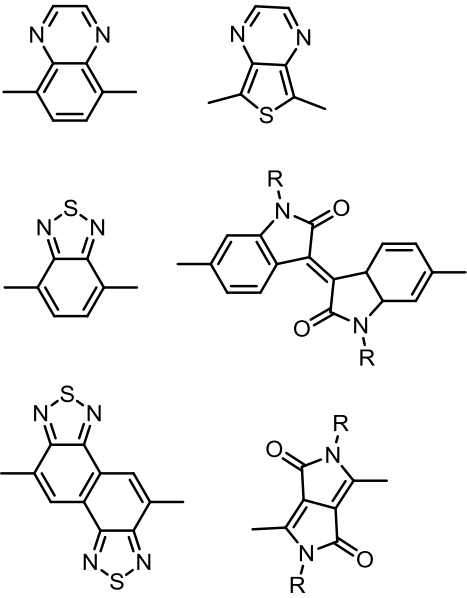
Figure 12. Schematic representation of a) p-doping and b) n-doping process

Upon applied positive or negative potential to the polymer, a partially delocalized radical cation or a radical anion is generated and named as polaron. A further redox process causes the formation of a bipolaron. Bipolaron can be formed by either further oxidation of polaron or combination of two polarons. Polarons and bipolarons are mobile through polymer backbone and ensure conductivity.

3.3. Benzotriazole and Benzothiadiazole Bearing Conjugated Polymers
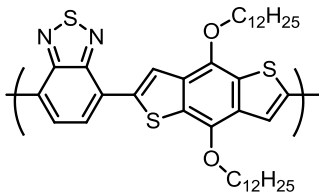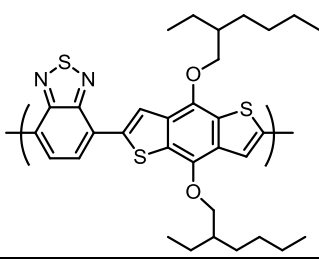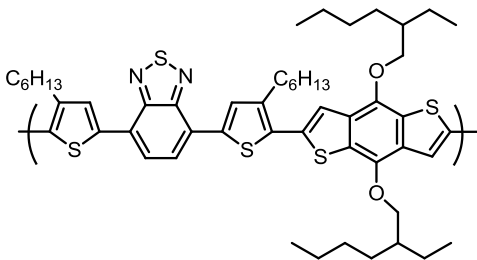
Electron deficient groups are called as acceptor units which are divided into three categories according to electron-accepting ability. They are shown in Table 1.[31] It is worth to mention that all most all of them contain electron-withdrawing imine (–C=N) bond. Generally, electron-accepting ability is associated with LUMO energy level of the material. In this manner, stronger acceptor refers to a material which has lower LUMO energy level.

Table 1. Common Acceptor Units

Weak Acceptor	Medium Acceptor	Strong Acceptor

D-A type polymers are frequently used in conjugated polymers in order to achieve high PCE. Selection of donor and acceptor units is important for absorption, energy levels and PCE. It is known that benzothiadiazole (BT) is one of the strongest acceptor moieties. After first synthesis of brominated BT in 1970[32], the first BT bearing D-A polymer was synthesized in 1996.[33] Following by these success, there have been a lot of polymer synthesized based on BT and they are used to construct OSCs.[34,35] This unit is frequently used in polymers with benzodithiophene donor moiety in the literature. Some examples from the literature[36,37,38] are given in Table 2.

Table 2. Examples of the benzothiadiazole containing polymers

Polymer	PCE %	Reference
	0.90	Reference 36
	1.19	Reference 37
	1.86	Reference 38

Due to of the more electron rich "N" atom, benzotriazole (BTz) is a weaker acceptor compared to BT. However, it has solubility advantage because it can incorporate an alkyl chain. This advantage brings polymer solution processability. It is also frequently used for organic solar cell applications. Examples of them[39,40,41,42] are shown in Table 3.
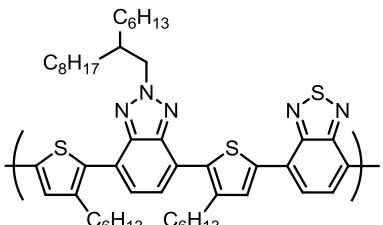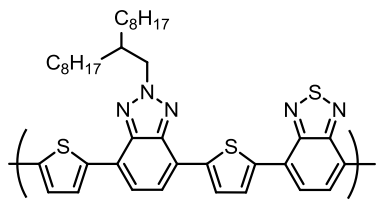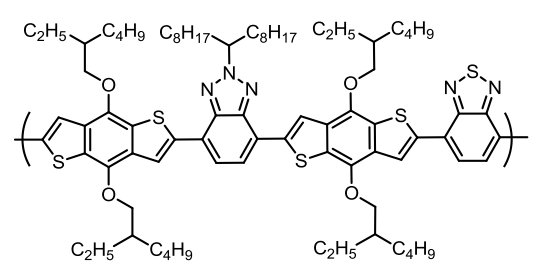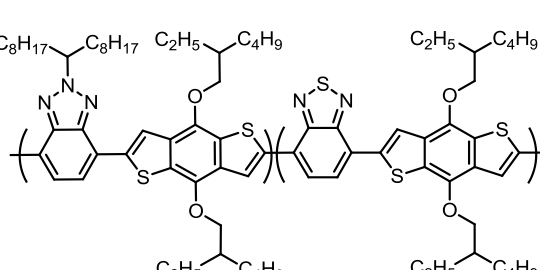
Table 3. Examples of the benzotriazole containing polymers

Polymer	PCE %	Reference
	1.4	Reference 39
	1.95	Reference 40
	2.12	Reference 41
	3.60	Reference 42

To combine these two units advantageous, since they can be in the same polymer backbone together.[43,44] In 2013, Kotowski and coworkers synthesize four polymers (Table 4) containing BT and BTz units.[45] Among those, the PCE % of the polymers which have thiophene as co-unit was quite low. When they replaced thiophene with benzodithiophene (BDT) unit, they got some advantages such as enhanced blend morphology and lower optical energy band gap. However, probably low molecular weight causes low PCE %. After this observation, they decided to change sequence

alternating to random. Thus, high molecular weight with good solubility was obtained and PCE % was reached from 1.48 to 5.01.

Table 4. Examples of the benzotriazole and benzothiadiazole containing polymers

Polymer	PCE %	Reference
	1.88	Reference 45
	0.26	Reference 45
	1.48	Reference 45
	5.01	Reference 45

3.4. Effect of Fluorination on Conjugated Polymers

When designing polymers for better optoelectronic properties, several groups focused on enhancing V_{oc}, J_{sc} and FF values with backbone fluorination.[46,47,48] Zhou and coworkers published the first fluorinated BT and demonstrated that it exhibited better device performance relative to the nonfluorinated BT polymer in OSC.[49]

Fluorine atom is the most electronegative element and the smallest electron-withdrawing group. Thus, replacing H atom with F atom does not cause steric hindrance due to small size, while it causes downshifted HOMO and LUMO levels and enhanced V_{oc} value. Stuart et al. also showed that fluorination improve J_{sc} and FF values due to reducing charge recombination.[50] Moreover, fluorine atom can construct inter or intramolecular interaction through F…H, F…F and F…S interactions.[51]

3.5. Aim of the Thesis

The main aim of this study is to synthesize new polymers with broad absorption and suitable band gap for OSC applications. Nonfluorinated and fluorinated benzothiadiazole containing two polymers were compared in order to investigate effect of fluorination to HOMO and LUMO energy levels, V_{oc}, and PCE values. Also, BTz unit brought these polymers solubility with branched alkyl chain and BDT unit was chosen as donor moiety. Both two polymers were synthesized with Stille coupling reaction. Structures of the polymers are given below in Figure 13.
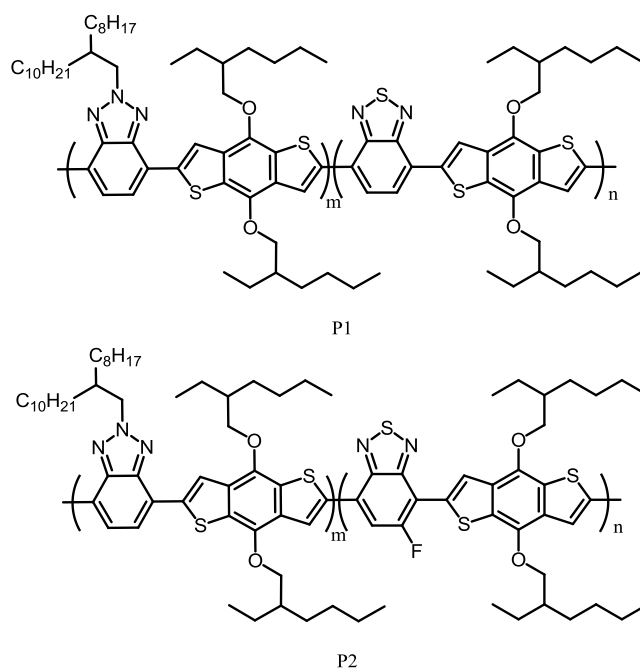
Figure 13. Structures of the polymers designed and synthesized for this study

CHAPTER 4

EXPERIMENTAL

4.1. Materials and Equipments

All chemicals and solvents were purchased from Sigma Aldrich Chemical Co. Ltd. Triethylamine, toluene and THF were distilled under nitrogen atmosphere before use. For purification step with column chromatography, Merck Silica Gel 60 was used. To verify structure of monomers, nuclear magnetic resonance (NMR) spectra were investigated on a Bruker Spectrospin Avance DPX-400 Spectrometer with internal reference as trimethylsilane (TMS) in deuterated chloroform ($CDCl_3$). Electrochemical studies were performed with Gamry 600 potentiostat, and an Agilent 8453 spectrometer was used for spectroelectrochemical measurements. OSC device fabrication and characterization were achieved in a glove box system (MBraun). Evaporations of cathode and LiF layers were provided with INFICON SQC-310 Thin Film Deposition Controller. A Perkin Elmer Differential Scanning Calorimetry was used for Differential Scanning Calorimetry (DSC), and a PerkinElmer Pyris 1 TGA was used for thermal gravimetry analyses (TGA) at a heating rate of 10°C/min under nitrogen atmosphere.

4.2. Synthesis

4.2.1. Syntheses of Monomer
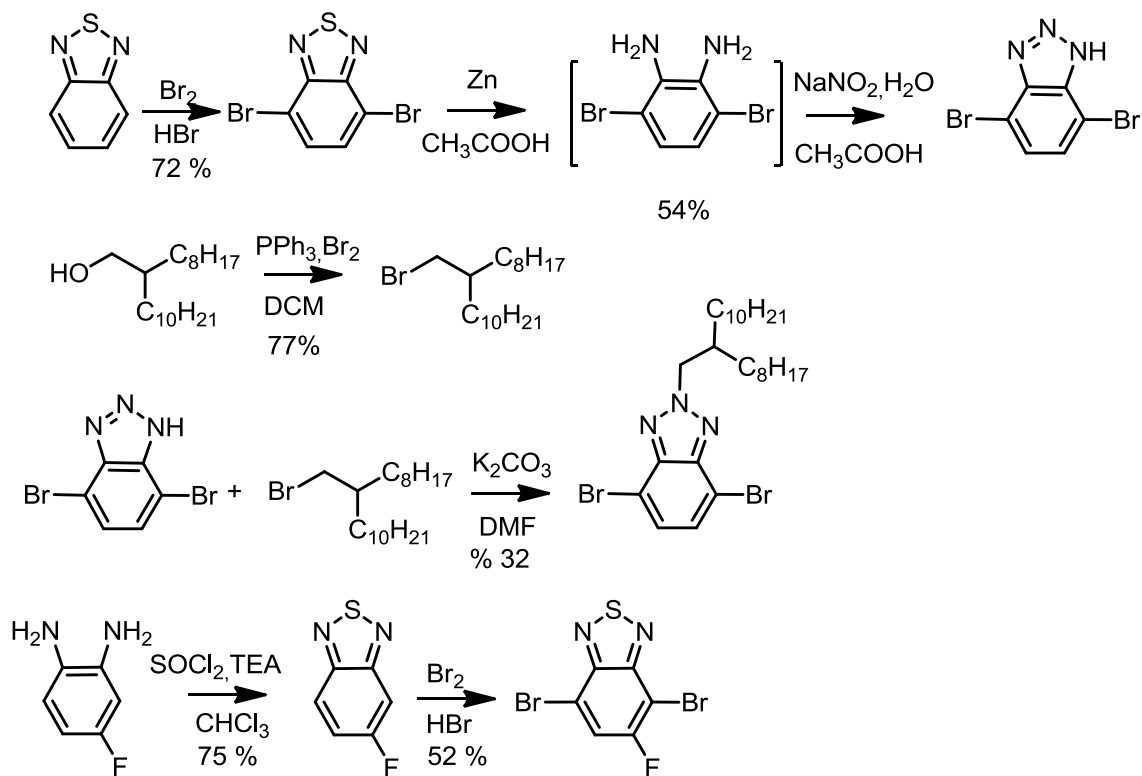
Figure 14. Synthetic pathway of the monomers

4.2.1.1. Synthesis of 9-(bromomethyl)nonadecane [52]
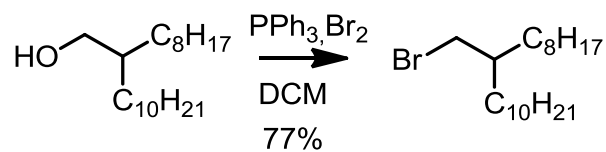
Figure 15. Synthesis of 9-(bromomethyl)nonadecane

2-Octyldodecan-1-ol (5.00 g, 16.75 mmol) was dissolved in 30 mL dichloromethane (DCM) and triphenylphosphine (PPh_3) (4.60 g, 17.59 mmol) was added to solution in

one portion at 0°C. Bromine (Br$_2$) (2.04 mL, 39.68 mmol) in 10 mL DCM was added drop wise to the solution. After addition, reaction was stirred at room temperature for 4 hours. After reaction was completed, the excess of Br$_2$ was quenched with adding saturated NaHSO$_3$ solution. Then, the mixture was extracted with DCM and brine. Organic part was dried with magnesium sulfate (MgSO$_4$) and its solvent was evaporated. Column chromatography was performed to obtain colorless oil. Yield: 77%

^{1}H NMR (400 MHz, CDCl$_3$) δ 3.44 (d, J = 4.7 Hz, 2H), 1.63 – 1.57 (m, J = 5.4 Hz, 1H), 1.40 – 1.21 (m, 32H), 0.88 (t, J = 6.7 Hz, 6H).

^{13}C NMR (101 MHz, CDCl$_3$) δ 39.65, 39.52, 32.57, 31.93, 29.80, 29.65, 29.60, 29.56, 29.36, 29.31, 26.57, 22.70, 14.11.

4.2.1.2. Synthesis of 4,7-dibromo-2,1,3-benzothiadiazole [52]
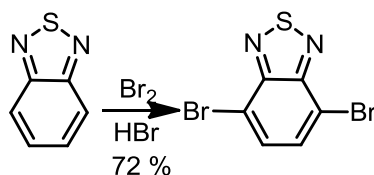
Figure 16. Synthesis of 4,7-dibromo-2,1,3-benzothiadiazole

2,1,3-Benzothiadiazole (2.50 g, 18.36 mmol) was stirred in 30 mL hydrobromic acid (HBr) for 1 hour. Br$_2$ (2.80 mL, 55.07 mmol) and 15 mL HBr mixture were added to the reaction slowly. It was refluxed at 120°C for 16 hours. After addition of saturated NaHSO$_3$ solution, mixture was poured into water. Precipitate was washed with cold diethyl ether. After drying, a yellow product was obtained. Yield: 72 %

^{1}H NMR (400 MHz, CDCl3) δ 7.72 (s, 1H).

^{13}C NMR (101 MHz, CDCl$_3$) δ 152.95, 132.33, 113.91.

4.2.1.3. Synthesis of 5-Fluoro-2,1,3-benzothiadiazole [53]
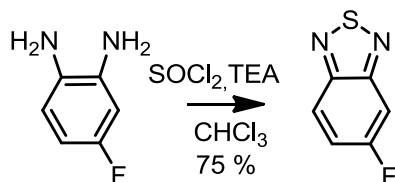
Figure 17. Synthesis of 5-Fluoro-2,1,3-benzothiadiazole

4- Fluoro-1,2-phenylamine (1.01 g, 7.93 mmol) was dissolved in chloroform (CHCl$_3$) (20 mL) and trimethylamine (4.4 mL, 31.71 mmol) mixture. After the mixture was cooled to 0°C, thionyl chloride (1.16 mL, 15.85 mmol) was added slowly. Then, the reaction was stirred at 70°C for 7 hours. The mixture was allowed to cool to room temperature and extracted with DCM and water. Organic layer was dried over MgSO$_4$ and solvent was removed. The product was purified by column chromatography on silica gel (hexane / DCM: 1 /3). Yield: 75 %

^{1}H NMR (400 MHz, CDCl$_3$) δ 7.98 (dd, J = 9.5, 5.2 Hz, 1H), 7.61 (dd, J = 8.8, 2.5 Hz, 1H), 7.43 (ddd, J = 9.5, 8.6, 2.5 Hz, 1H).

^{13}C NMR (101 MHz, CDCl$_3$) δ 164.78, 162.26, 154.79, 152.01, 122.59, 122.48, 121.49, 121.20, 104.92, 104.69.

4.2.1.4. Synthesis of 4,7-Dibromo-5-fluoro-2,1,3-benzothiadiazole [54]
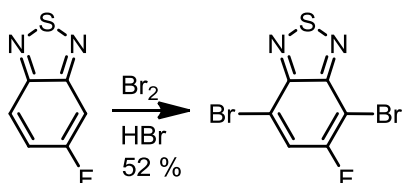
Figure 18. Synthesis of 4,7-Dibromo-5-fluoro-2,1,3-benzothiadiazole

Br$_2$ (2.3 mL, 45.4 mmol) in 10 mL HBr was added slowly into 5-fluoro-2,1,3-benzothiadiazole (0.70 g, 4.54 mmol) and HBr (20 mL) mixture. Then, the reaction was heated at 120°C for 2 days. After the reaction was completed, saturated NaHSO$_3$ solution was added. The mixture was poured into water and solid was filtered. After recrystallization of it with ethanol, the product was obtained as yellow solid. Yield: 52%

^{1}H NMR (400 MHz, CDCl$_3$) δ 7.78 (d, J = 8.3 Hz, 1H).

^{13}C NMR (101 MHz, CDCl$_3$) δ 158.94, 156.40, 150.35, 150.28, 147.87, 121.59, 121.27, 111.60, 111.49, 95.88, 95.64.

4.2.1.5. Synthesis of 4,7-Dibromo-1H-benzotriazole [55]
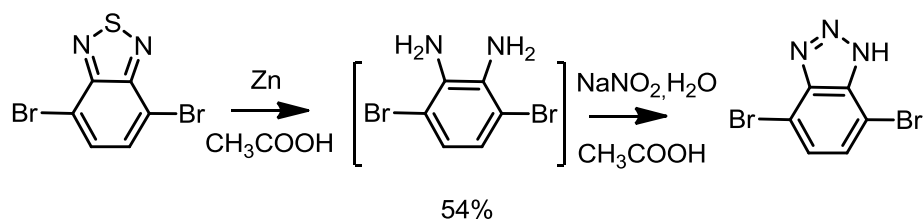
Figure 19. Synthesis of 4,7-Dibromo-1H-benzotriazole

4,7-Dibromo-2,1,3-benzothiadiazole (2.50 g, 8.50 mmol) was dissolved in acetic acid/water (25 mL/25 mL) mixture under nitrogen atmosphere. Then, zinc dust (5.56 g, 85 mmol) was added to reaction medium in small portions. After stirring at 70°C for 5 hours, reaction was finished by TLC control and allowed to cool. The reaction mixture was filtered to remove excess zinc dust. Sodium nitrite (0.60 g, 8.50 mmol) in 10 mL water was poured into the filtrate. It was allowed to stirring for 30 minutes at room temperature. Cold water added to the reaction and the mixture was filtrated to collect the precipitate. The product was obtained by washing with water several times as 1.27 g. Yield : 54%

^{1}H NMR (400 MHz, CDCl$_3$) δ 7.51 (s, 2H).

4.2.1.6. 4,7-dibromo-2-(2-octyldodecyl)-benzotriazole [56]
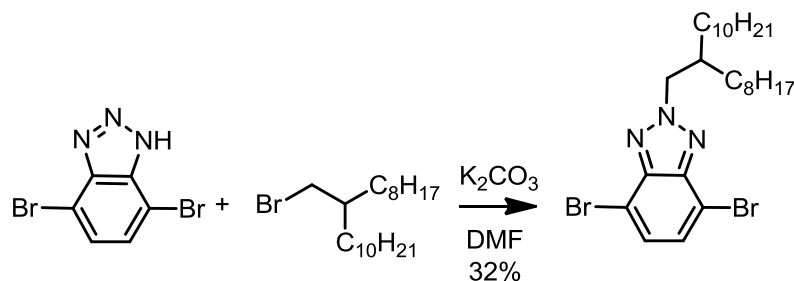
Figure 20. Synthesis of 4,7-dibromo-2-(2-octyldodecyl)-benzotriazole

4,7-Dibromo-1H-benzotriazole (0.60 g, 2.17 mmol) and 9-(bromomethyl) nonadecane (0.94 g, 2.60 mmol) was dissolved in 6 mL dry dimethylformamide in round-bottomed flask. After dissolving of them, potassium carbonate (1.20 g, 8.68 mmol) was added in one portion. The temperature of the reaction mixture was brought to 90°C and stirred 5 hours at this temperature. Then, reaction mixture was poured into 800 mL brine, and extracted with diethlyl ether. Following the evaporation of solvent, column chromatography (2 Hexane: 1 Chloroform) yielded a yellow oil product. Yield: 32 %

^{1}H NMR (400 MHz, CDCl$_3$) δ 7.38 (s, 2H), 4.65 (d, J = 7.2 Hz, 2H), 2.35 – 2.26 (m, 1H), 1.32 – 1.13 (m, 32H), 0.84 (td, J = 6.9, 3.3 Hz, 6H).

^{13}C NMR (101 MHz, CDCl$_3$) δ 143.65, 129.43, 110.00, 61.16, 39.02, 31.91, 31.86, 31.16, 29.77, 29.60, 29.58, 29.46, 29.42, 29.33, 29.24, 26.02, 22.68, 22.66, 14.12.

4.2.2. Synthesis of Poymers
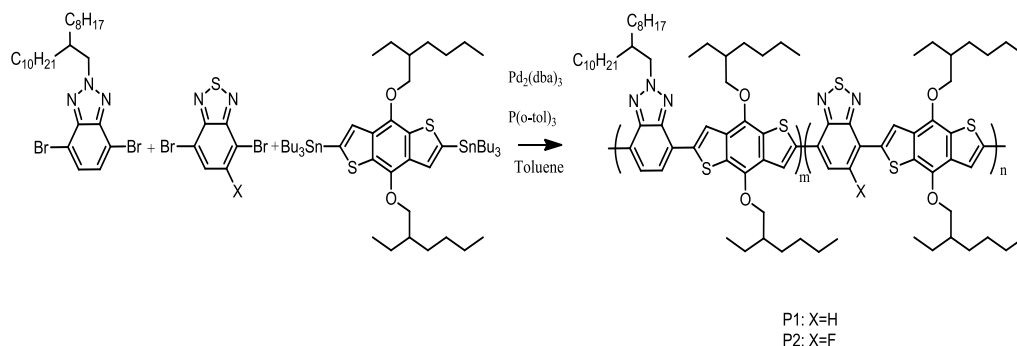
Figure 21. General synthetic pathway for the polymers

4.2.2.1. Synthesis of P1 [45]
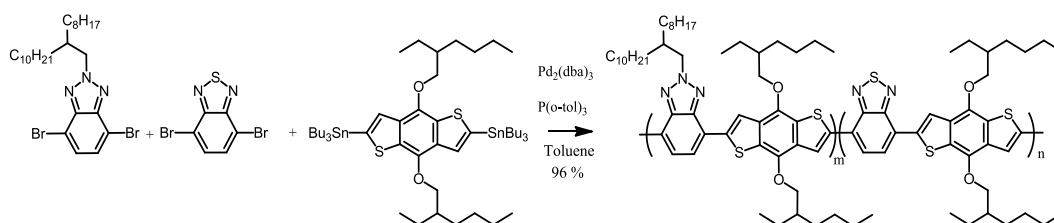
Figure 22. Synthesis of **P1**

(4,8-Bis((2-ethylhexyl)oxy)benzo[1,2-b:4,5-b']dithiophene-2,6diyl)bis(tributyl-stannane) (250 mg, 0.324 mmol), 4,7-dibromo-2,1,3-benzothiadiazole (47 mg, 0.162 mmol), 4,7-dibromo-2-(2-octyldodecyl)-benzotriazole (90 mg, 0.162 mmol) were placed in two-necked round bottom flask and dissolved in 10 mL toluene under nitrogen atmosphere. Reaction mixture was deoxygenated by bubbling with nitrogen for 45 minutes. Then, tris(dibenzylideneacetone)dipalladium (7.4 mg, 8.09×10^{-3} mmol) and tri(o-tolyl)phosphine (19 mg, 6.47×10^{-2} mmol) were added and the reaction mixture was stirred at 110°C for 40 hours. 2-(Tributystannyl)thiophene and 2-bromothiophene were used as the end-capping agents. After removal of toluene under reduced pressure, the polymer was precipitated into methanol. The precipitate

was extracted in a Soxhlet apparatus with acetone, hexane and chloroform. The polymer which recovered by chloroform was precipitated into methanol and obtained as blue solid (222mg, yield: 96%). Mn: 52600, Mw: 124400, PDI= 2.36

4.2.2.2. Synthesis of P2 [45]
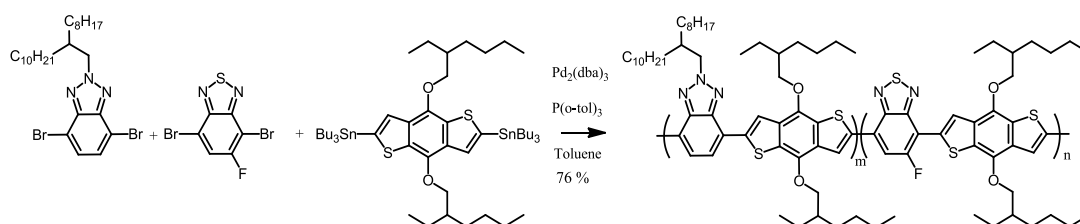
Figure 23. Synthesis of **P2**

The same procedure was performed for **P2** using (4,8-bis((2-ethylhexyl)oxy)benzo[1,2-b:4,5-b']dithiophene-2,6-diyl)bis(tributylstannane) (277 mg, 0.359 mmol), 4,7-dibromo-2,1,3-benzothiadiazole (56 mg, 0.179 mmol), 4,7-dibromo-2-(2-octyldodecyl)-benzotriazole (100 mg, 0.179 mmol). A blue polymer was obtained as 0.197 mg. Yield: 76%. Mn: 42800, Mw:112000, PDI= 2.62

4.3. Characterization of Conjugated Polymers

4.3.1. Cyclic Voltammetry

Cyclic voltammetry (CV) is a very common tool to study electrochemical behavior of CPs. It is useful for both electrochemical synthesis and characterization of them. It gives some qualitative information about CPs like p- or n- type doping and dedoping potentials, and reversibility of process.

In cyclic voltammetry set up, there are three different electrodes: Working electrode (WE), reference electrode (RE), and counter electrode (CE). The desired potential is applied to WE with respect to RE via potentiostat. The major current which is generated in this process passes between CE and WE. Three electrodes are placed in a cell which is charged with solvent-supporting electrolyte mixture. This solvent should not react with electrodes and should dissolve the supporting electrolyte. The

purpose of adding supporting electrolyte to the solution is to provide ionic conductivity. Before an experiment, the potential range is determined by a background run which is a measurement in the presence of bare WE, CE, RE, supporting electrolyte, and solvent. This potential range depends on their potential window. Experimental setup of CV analysis is given in Figure 24.
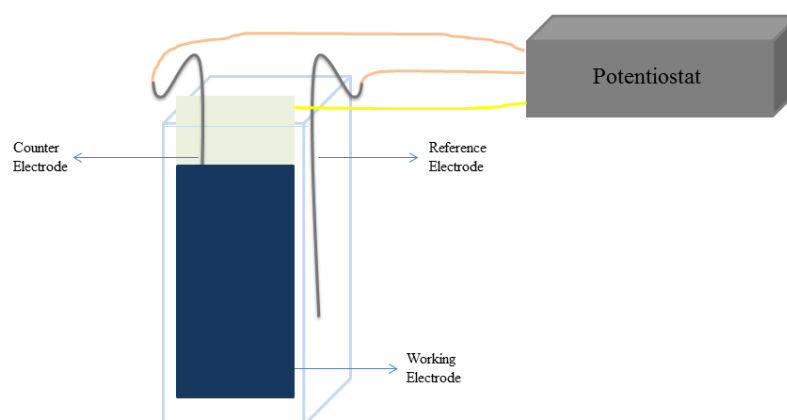
Figure 24. Cyclic voltammetry analysis experimental setup

4.3.2. Spectroelectrochemistry

Spectroelectrochemistry is combination of two important methods: Electrochemistry and spectroscopy. For this purpose a three electrode system is constructed in a UV cuvette. It gives a chance of measuring absorption upon supplying oxidative or a reductive potential. Thus, change in absorption can prove color change during doping process. From the resultant spectra λ_{max} and optical bang gap can be calculated and also formation of polaron and bipolaron bands can be observed. Figure 25 illustrates a spectroelectrochemistry analysis setup.
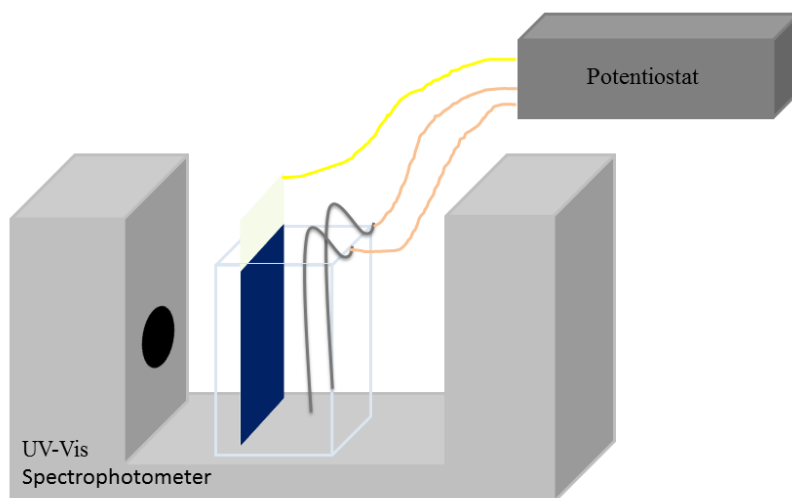
Figure 25. Spectroelectrochemical analysis experimental setup

4.3.3. Kinetic Study

Kinetic study is a useful technique to determine optical contrast and switching time which are important parameters for electrochromic polymers. Optical contrast is the percent transmittance change between the neutral and fully oxidized states of a material at a given wavelength. The time required for switching between these states is defined as the switching time. In the literature, switching time is calculated from 95% of the full contrast since human eye is insensitive to 5% of color change.[57] Another parameter is coloration efficiency (CE) which is defined as the proportionality factor that relates the optical absorbance change at a specific wavelength to the change in electrochemical charge to required switch between two states.

When square wave potential applied between neutral and oxidized state at a specific wavelength, absorption change is monitored by UV-Vis spectroscopy. The specific wavelength is determined from the electronic spectra where shows maximum absorbance. Experimental setup of kinetic study is same with spectroelectrochemical analysis setup.

4.3.4. Colorimetry

To observe a color change upon applied potential to a conjugated polymer, a scientific methodology is required. Color of a material can be described with three main characters; hue, saturation, and luminance. The CIE system specifies color confidently and depends on CIE color spaces such as CIE XYZ (1931), CIE YUV (1960), CIE Yu'v' (1976), and CIE L*a*b*(1976).[58]

4.3.5. Organic Solar Cell Study

Construction of ITO/PEDOT:PSS/ Polymer:$PC_{70}BM$/LiF/Al devices consist of several steps. Firstly, ITO coated glass substrate are washed with toluene, detergent and water, acetone and isopropyl alcohol in order to get rid of impurities. Plasma cleaning is performed for 5 minutes with Harrick Plasma Cleaner. PEDOT:PSS is applied on ITO by spin coating at 3500 rpm for 45 minute. Then, substrates are dried on heater 135 °C for 15 minutes. In a glove box, polymer: $PC_{70}BM$ mixture is applied at 750 rpm. Then, LİF(0.6 nm) and Al (100 nm) layers are coated through a shadow mask by evaporation of them under vacuum of 2×10^{-6} mbar (Figure 26). After measuring of active area, characterization of devices is achieved using a Keithley 2400 source meter under AM 1.5G irradiation (100 mV/cm^2).
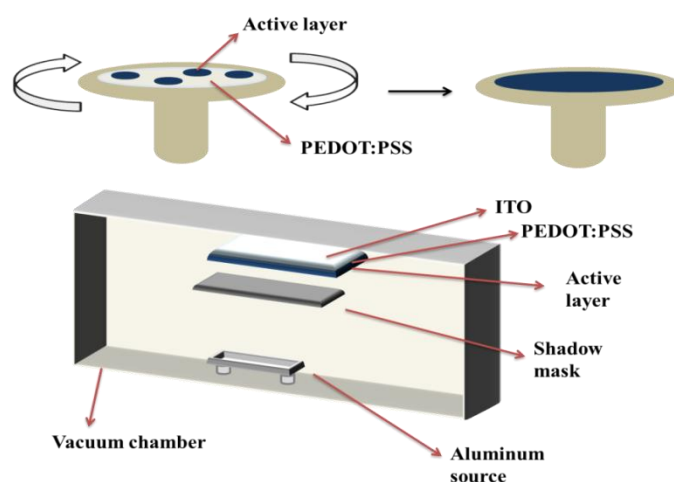
Figure 26. Application of layers in OSC

CHAPTER 5

RESULTS AND DISCUSSIONS

5.1. Electrochemical Studies

In order to determine whether the polymers are suitable for OSC applications or not, electrochemical studies were performed. As mentioned above, HOMO and LUMO energy levels are critical for charge transportation in OSC. To investigate these values, CV method was used. Polymers were dissolved in chloroform and the solutions were applied to ITO surface by using a spray gun. Polymer coated ITO (WE), Pt wire (CE), and Ag wire (RE) were placed in a cell which contains 0.1 M tetrabutylammonium hexafluorophosphate/acetonitrile (TBAPF$_6$/ACN) mixture. Cyclic voltammograms were monitored between 0 V-1.3 V for **P1** and **P2** at a scan rate of 100 mV/s at room temperature. It can be said that both polymers can be doped only upon positive potential which are shown in Figure 27.
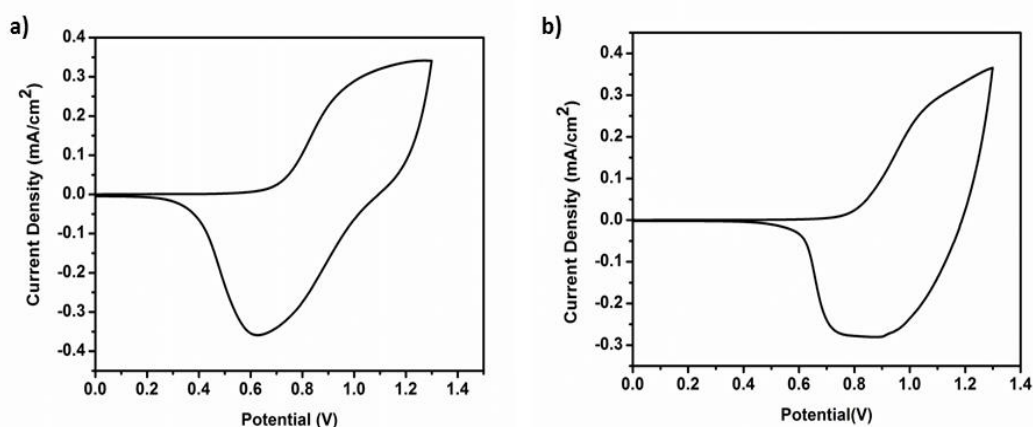
Figure 27. Cyclic voltammograms of a) **P1**, b) **P2** in 0.1 M TBAPF$_6$/ACN at 100mV/s scan rate

P1 and **P2** have 0.98 V/0.63 V and 1.07 V/0.85 V redox couples respectively. The difference between oxidation potential of the polymers can be attributed to electron withdrawing nature of the fluorine atom. Electron density on **P2** chain is decreased because it contains fluorinated benzothiadiazole. Thus, doping/dedoping processes can occur at a higher oxidation potential.

Cyclic voltammetry studies also give information about HOMO and LUMO energy levels which are calculated from onset potentials of oxidation and reduction according to following equations (SHE vs vacuum level was taken as 4.75 eV);

$$HOMO = -(4.75 + E_{ox}{}^{onset})$$

$$LUMO = -(4.75 + E_{red}{}^{onset})$$

Since both polymers showed only p-dopable character, only HOMO energy levels of the polymers could be calculated from the cyclic voltammetry studies as -5.45 eV and -5.55 eV for **P1** and **P2** respectively. This was an expected result, because in the literature it was known that addition of fluorine atom decreases HOMO and LUMO energy levels.[59,60] Moreover, LUMO energy levels were calculated by using the optical band gap which was calculated in spectroelectrochemical part. According to the formula of $E_g = E_{HOMO} - E_{LUMO}$, LUMO levels were found as -3.67 eV for **P1** and -3.83 for **P2**. The results of CV analysis were summarized in Table 5.

Table 5. Summary of Electrochemical Study of **P1** and **P2**

Polymer	$E_{p\text{-doping}}$ (V)	$E_{p\text{-dedoping}}$ (V)	$E_{ox}{}^{onset}$(V)	HOMO(eV)	LUMO(eV)
P1	0.98	0.63	0.70	-5.45	-3.67
P2	1.07	0.85	0.80	-5.55	-3.83

The results obtained from the CV studies showed that both polymers are proper candidates for the OSC applications. Their energy levels are given in Figure 28.
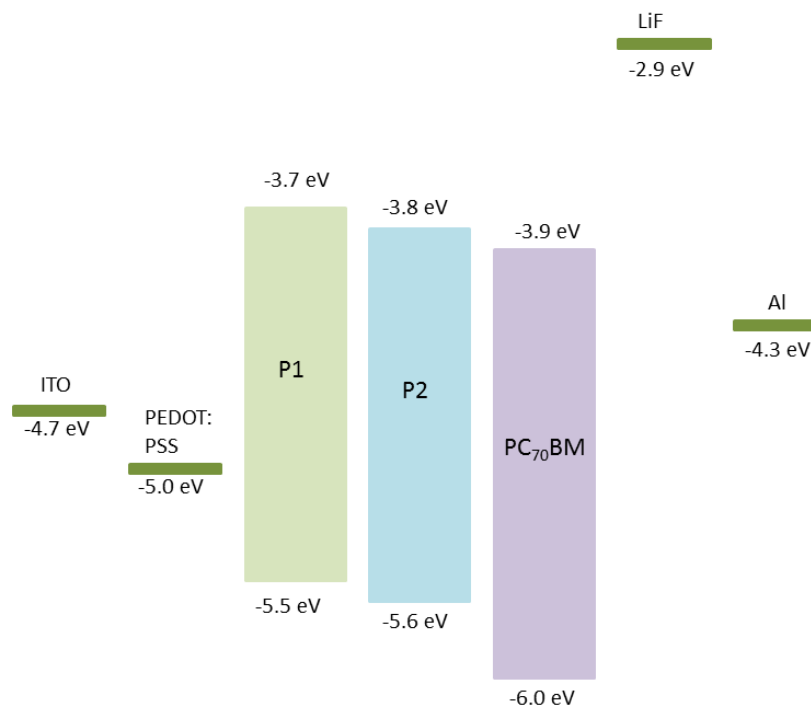
Figure 28. Energy level diagram of the **P1** and **P2**

5.2. Spectroelectrochemistry Studies

Absorption in visible and NIR regions was investigated by spectrophotometer. Polymer coated ITO film was prepared with spray coating and used for thin film measurements. For solution spectra, polymers were dissolved in chloroform. As seen in Figure 29, both polymers had broad absorptions in visible region. Each showed a peak at 575 nm with a shoulder at 615 nm for **P1** and 635 nm for **P2** in thin film. While shorter wavelength absorption can be assigned to π-π* transition, absorption at longer wavelength can be assigned to intramolecular charge transfer (ICT) between the electron-rich and electron-deficient units.[61] The absorption spectra of the polymers were similar and this similarity between fluorinated and nonfluorinated polymers was previously reported in the literature.[62,63] However, broader absorption in the fluorinated polymer effected λ_{max}^{onset} value and so optical band gap.
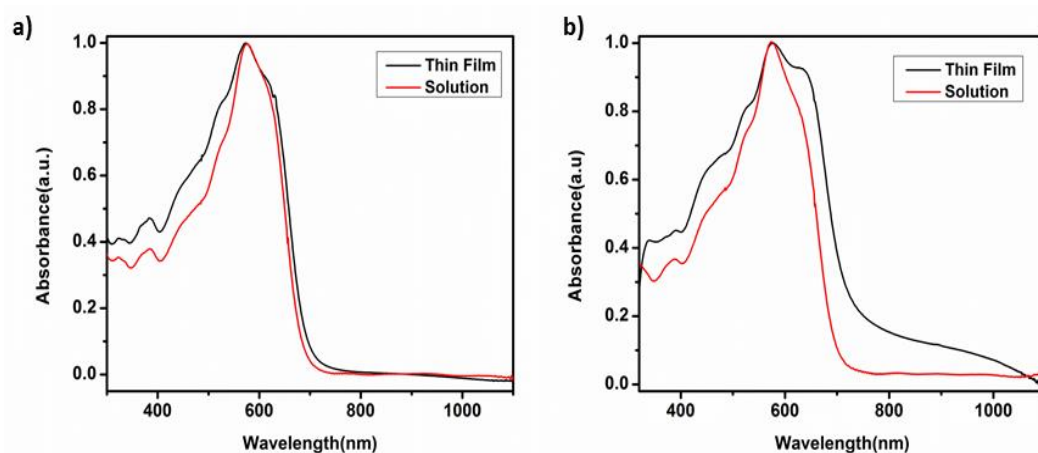
Figure 29. UV-vis normalized absorption spectra of in $CHCl_3$ solution and film for (a) **P1**, (b) **P2**

Optical band gaps were determined from the λ_{max}^{onset} values which were 695 nm for **P1** and 720 nm for **P2**. Thus, the optical band gaps of the polymers were calculated according to equation which was given below:

$$E = hv = \frac{hc}{\lambda}$$

where

h: Planck's constant (6.626×10^{-34} J·s)

c: the speed of light (2.998×10^{8} m.s^{-1})

In this formula, when these values are written in electron volt (eV) unit, the equation becomes to;

$$E = \frac{1241}{\lambda}$$

Thus, 1.78 eV and 1.72 eV was found as the optical band gaps for **P1** and **P2** respectively. This implies that fluorination to the polymer backbone lowered LUMO level more than HOMO level and cause to slightly narrow band gap than **P1**.

Table 6. Summary of the optical studies of the polymers

Polymer	λ_{max} (nm)	λ_{max}^{onset} (nm)	E_g^{op} (eV)
P1	575/615	696	1.78
P2	575/635	720	1.72

After bringing the polymers to their neutral states, the polymer films were exposed to stepwise oxidation potential (Figure 30). For this experiment, 0.1 M TBAPF$_6$/ACN were taken in a quartz cell with three electrode system which consists of RE (Ag), CE (Pt), and WE (polymer coated ITO). It is clearly observed that, when there was a decrease in the intensity of absorption of neutral state, formation of polaron bands around 800 nm for both polymers was observed. It was also observed that **P1** and **P2** have isosbestic points where interconversion of the polymer from their neutral states to the oxidized states[64] at 656 nm and 678 nm respectively.
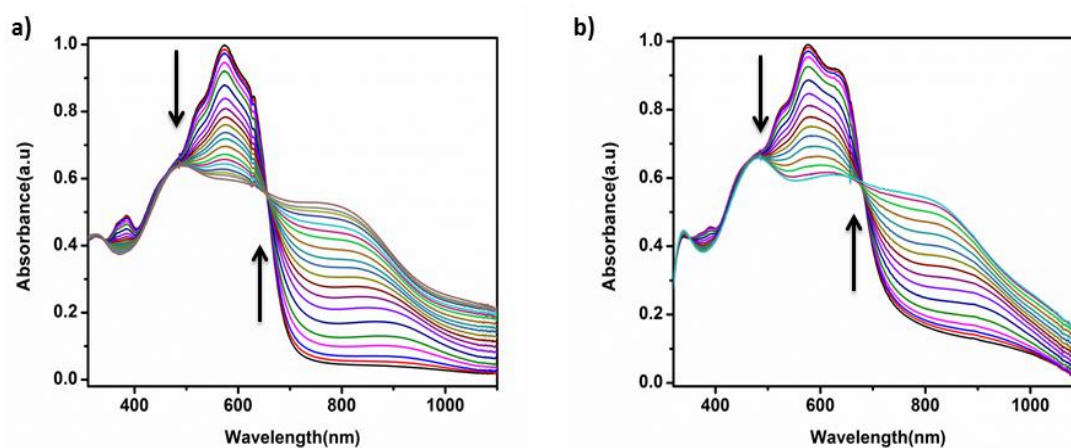

Figure 30. Electronic normalized absorption spectra of polymer films recorded at various potentials between 0 and 1.2 V for (a) **P1**, (b) **P2** in 0.1 M TBAPF$_6$/ACN solution

5.3. Kinetic Studies

Two important parameters for an electrochromic material namely optical contrast and switching time were determined by using combination of a potentiostat and a UV-Vis spectrophotometer. Three electrode system was constructed in a quartz cell as described for the spectroelectrochemistry part. Then, absorption spectrum was recorded by applying square-wave potential between neutral and fully oxidized states with 5 s time internals (Figure 31). This measurement was repeated for each wavelength which showed maximum absorption values in the absorption spectra of the polymers.
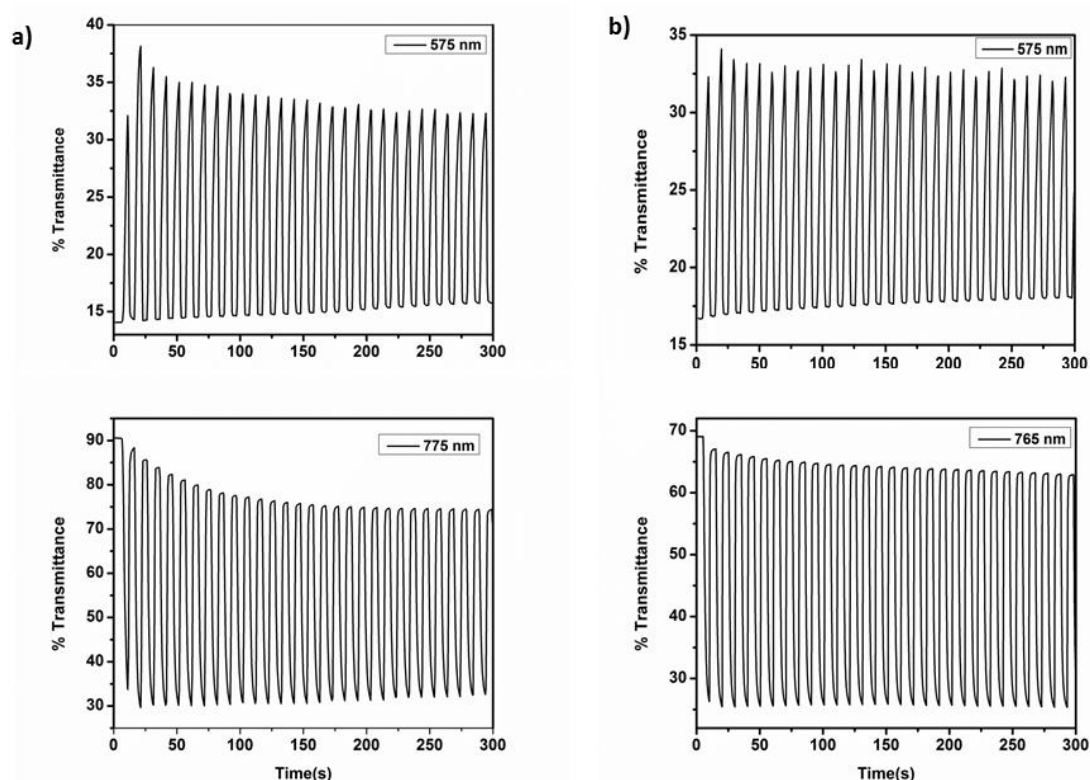

Figure 31. Percent transmittance changes of (a) **P1**, (b) **P2** in 0.1 M TBAPF$_6$/ACN solution

The optical contrast and switching times were reported in Table 7. It was expected that the optical contrast of **P1** would be higher than the optical contrast of **P2**

according to spectra of the polymers. Kinetic studies were in accordance with this expectation. On the other hand, the fastest switching time and highest coloration efficiency were observed for the **P2** with 0.6 s and 214 cm^2 C^{-1} respectively. These results showed that fluorine atom on the polymer backbone enhance switching time and coloration efficiency values. In the literature, it was mentioned that this behavior may be resulted from the efficient packing in the fluorinated polymers.[65]

Table 7. Summary of the kinetic studies of the polymers

Polymer	Wavelength(nm)	Optical Contrast (ΔT%)	Switching Time (s)	Coloration Efficiency (cm^2 C^{-1})
P1	575	24	3.6	116
	775	59	1.5	108
P2	575	17	4.2	109
	765	42	0.6	214

5.4. Colorimetry Studies

Similar structures and absorption spectra of the polymers caused to similar colors for the polymers. When they were dark blue in neutral state, their color of oxidized state were dark gray. These colors were correlated with absorption spectra at given potential at Figure 32.
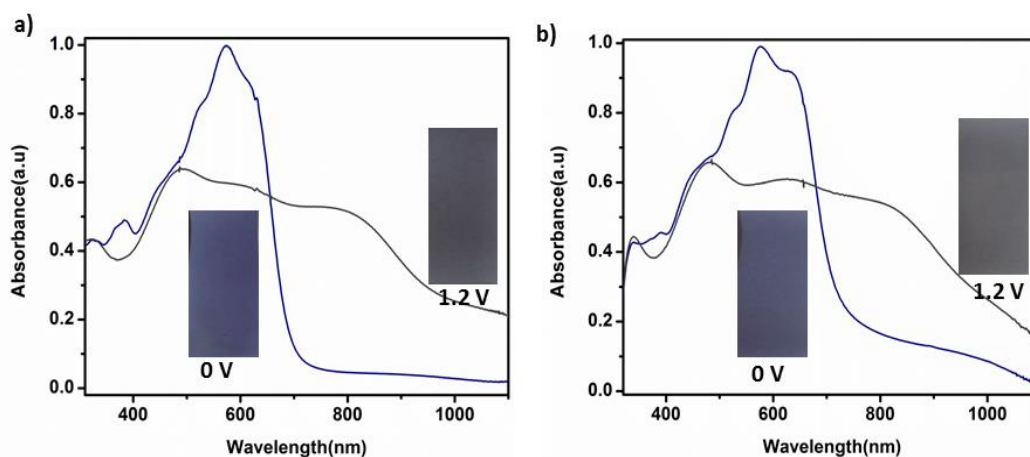
Figure 32. Colors in neutral and oxidized states of (a) **P1**, (b) **P2**

In order to report these colors in a scientific way, CIE coordinates were used and the colors were defined with luminance (L), hue (a) and saturation (b). When the color between red/magenta corresponds to a, the color between yellow and blue colors corresponds to b. L, a and b values of the polymers in neutral and oxidized states were given in the Table 8.

Table 8. Summary of colorimetric studies of the polymers

Polymer	Potential	L	a	b
P1	0 V	31	7	-21
	1.2 V	35	2	-5
P2	0 V	36	5	-16
	1.2 V	43	1	-3

5.5. Photovoltaic Studies

Bulk heterojunction OSCs were constructed according to ITO/PEDOT:PSS/ Polymer:$PC_{70}BM$/LiF/Al device configuration. ODCB was chosen as the solvent to prepare polymer: $PC_{70}BM$ blends since its high boiling point enables slow

evaporation. Slow evaporation process provides more-ordered structure and thus enhances morphology and device performance. Diiodooctane (DIO) was used as the additive during spin coating in order to reduce domain size by dispersing fullerene agglomerates.

In OSC device characterization, **P1** and **P2** polymers were blended with PCBM in various different donor:acceptor ratios by dissolving in ODCB. According to measurements, optimum polymer:fullerene ratios were determined as 1:3 for **P1** and 1:2 for **P2**. Nonfluorinated polymer **P1** had reasonable FF value as 54 % and showed maximum 2.41 % PCE for 1:3 ratio blend. Although FF and V_{oc} values were not affected significantly, J_{sc} was increased from 5 mA/cm^2 to 10 mA/cm^2 by adding DIO additive. Thanks to this improvement, the highest PCE for **P1** was calculated as 4.13%. The current density-voltage (J-V) graphs of OSCs for **P1** are depicted in Figure 33 and photovoltaic parameters are summarized in Table 9.
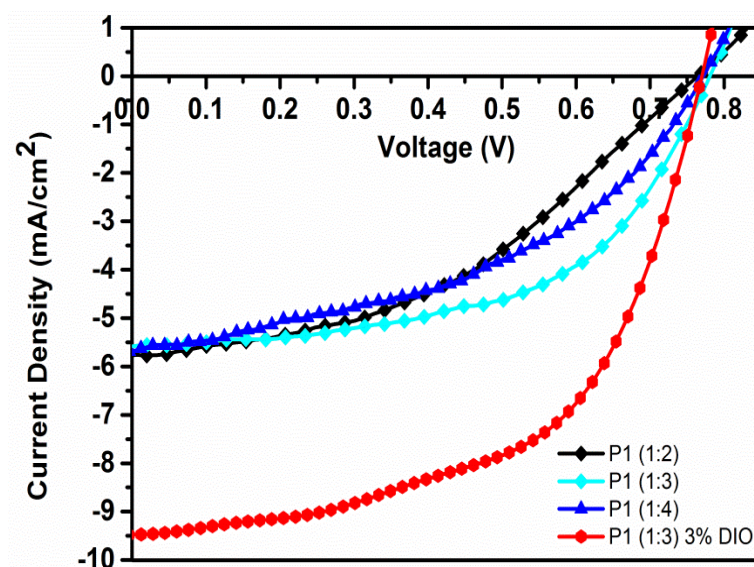

Figure 33. J-V characterization for **P1** donor-based OSCs

Table 9. Summary of device performance for **P1**

P1:PC$_{70}$BM (w:w)	J$_{sc}$ (mA/cm^2)	V$_{oc}$ (V)	J$_{max}$ (mA/cm^2)	V$_{max}$ (V)	FF%	PCE %	Treatment
1:2 (2%)	6.19	0.77	4.13	0.45	38.98	1.86	-
1:3 (2%)	5.67	0.78	4.30	0.56	54.52	2.41	-
1:4 (2%)	5.68	0.78	3.58	0.53	42.84	1.90	-
1:3 (3%)	4.83	0.76	3.17	0.39	38.73	1.42	-
1:3 (2%)	10.31	0.76	7.87	0.50	50.36	3.95	2% DIO
1:3 (2%)	**10.36**	**0.77**	**7.18**	**0.57**	**57.40**	**4.13**	**3% DIO**
1:3 (2%)	9.64	0.76	7.06	0.57	57.74	4.01	4% DIO

Kotowski et. al. reported that PCE of their random polymer which contains BT, BTz and BDT was maximum 2.63 % PCE without any additive.[45] This value is almost same with PCE of P1 of this study. However, when they applied CN additive, PCE was increased to 5.01 % which was higher than the highest PCE of P1. It might be said that CN additive cause to better device performance compared to DIO additive in BT, BTz and BDT bearing random polymer.

OSC studies also showed that adding fluorine atom to the polymer backbone increased J_{sc} from 5 mA/cm^2 to 9 mA/cm^2 without any additive and **P2** showed maximum 3.80 % PCE. It is interesting to note that while there was a decrease in HOMO value by backbone fluorination, V$_{oc}$ values of these two polymers were same. Li et. al. explained a similar case with decreased surface energy of fluorinated polymer.[66] Moreover, upon addition of DIO had an adverse impact on J_{sc} and FF values and caused a decrease in PCE. According to the literature, the reason of this case might be that fluorinated polymers could be more sensitive to processing conditions.[67] The current density-voltage (J-V) graphs of OSCs for **P2** are depicted in Figure 34 and photovoltaic parameters of them are summarized in Table 10.
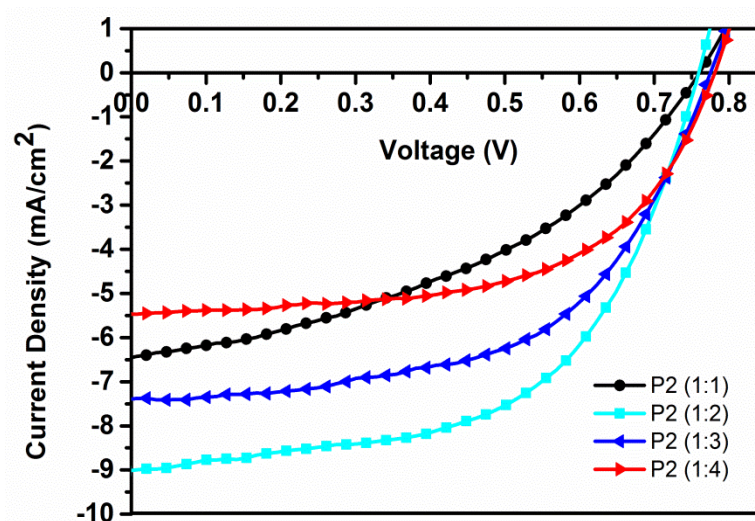
Figure 34. J-V characterization for **P2** donor-based OSCs

Table 10. Summary of device performance for **P2**

P2:PC$_{70}$BM (w:w)	J$_{sc}$ (mA/cm^2)	V$_{oc}$ (V)	J$_{max}$ (mA/cm^2)	V$_{max}$ (V)	FF%	Efficiency	Treatment
1:1 (2%)	6.46	0.77	3.90	0.52	40.76	2.03	-
1:2 (2%)	**9.40**	**0.77**	**7.04**	**0.54**	**52.50**	**3.80**	-
1:3 (2%)	7.43	0.78	5.68	0.57	55.81	3.23	-
1:4 (2%)	6.79	0.78	5.07	0.58	55.51	2.94	-
1:2 (3%)	8.41	0.78	5.98	0.54	49.18	3.23	-
1:2 (2%)	7.13	0.77	5.37	0.52	50.85	2.79	2% DIO
1:2 (2%)	6.83	0.76	4.11	0.42	33.24	1.73	3% DIO
1:2 (2%)	5.42	0.76	3.12	0.42	31.82	1.31	4% DIO

Incident photon to current efficiency (IPCE) gives the ratio of number of charges collected by electrodes to the number of incident photons. The highest IPCE values 34 % and 26 % for **P1** and **P2**, respectively (Figure 35).
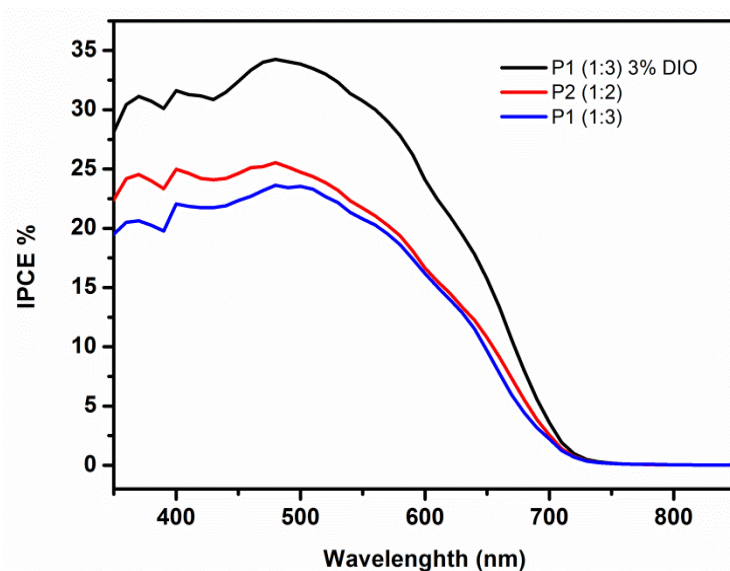

Figure 35. IPCE spectra for **P1** and **P2** donor-based devices

5.6. Morphology Studies

Differences in OSC performance of polymers were investigated with AFM analyses and given in Figure 36. These studies indicated that root-mean-square (RMS) values are 2.61 nm for **P1**, 4.62 nm for **P1**-additive, 1.94 nm for **P2**. It can be resulted that smoothest surface was observed in **P2**. The reason of this might be presence of intermolecular attraction because of H and F atoms in **P2**. The thickness of the active layer was 125 nm for **P1**, 138 nm **P1**-additive, and 136 nm for **P2**.
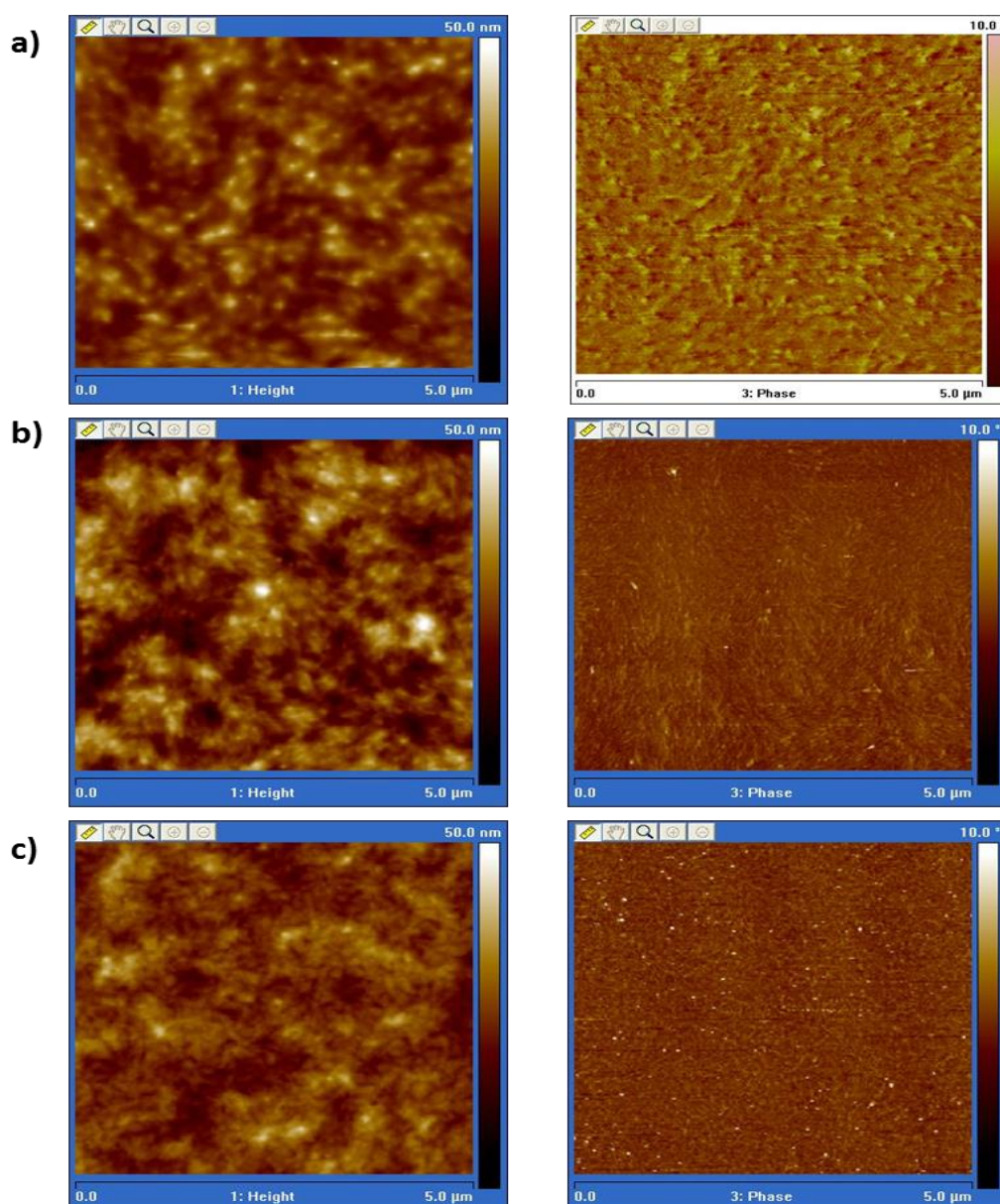
Figure 36. AFM height and phase images of (a) **P1**, (b) **P1** with additive, (c) **P2**

5.7. Thermal Studies

Differential scanning calorimetry (DSC) was used to determine thermal transitions (glass transition, melting, crystallization, curing). According to DSC curve of the **P1** (Figure 37) and **P2** (Figure 38), they did not show any significant degradation and any phase transition up to 300°C.
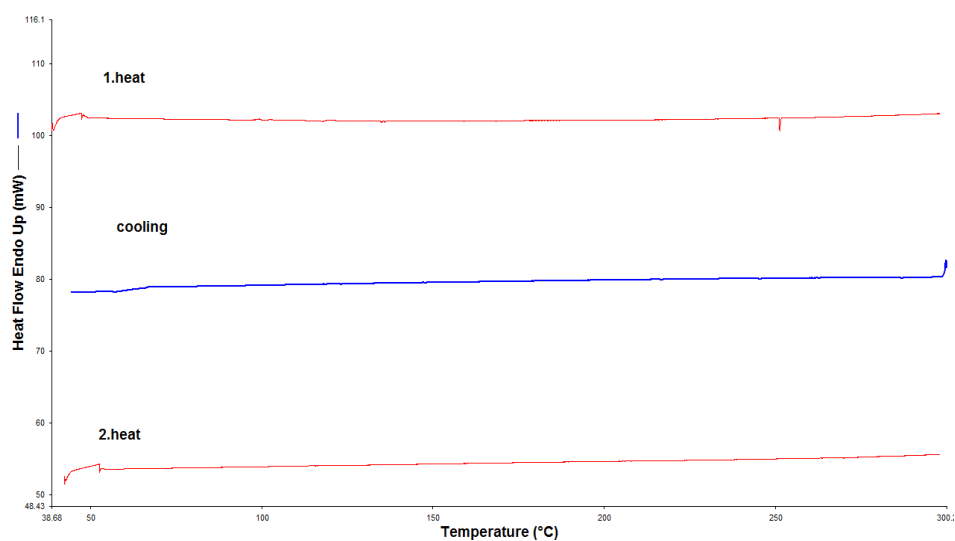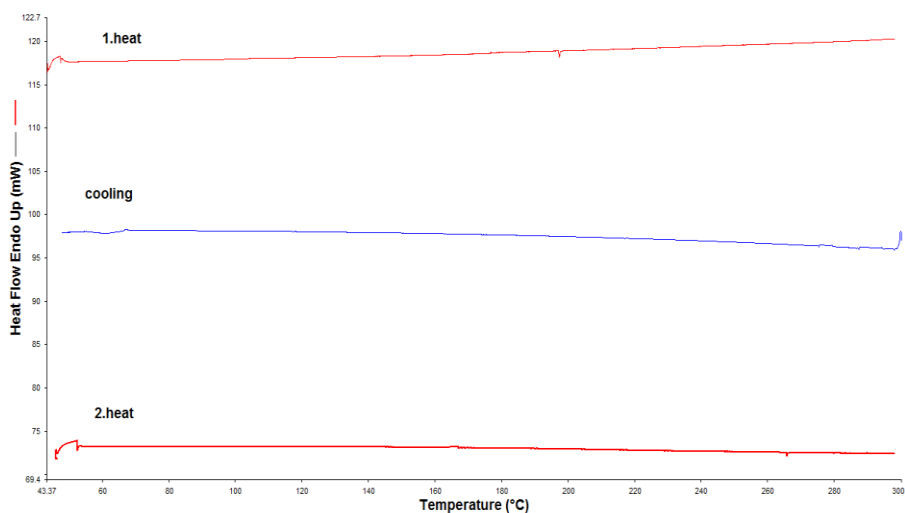
Figure 37. DSC study of **P1**

Figure 38. DSC study of **P2**

Thermal stability of the polymers was investigated with thermogravimetric analyses (TGA). These analyses showed that decomposition temperatures of **P1** (Figure 39) and **P2** (Figure 40) were 327°C and 322°C respectively. When 52% mass loss was observed for **P1**, 53% mass loss was observed for **P2** upon heating up to 650°C.
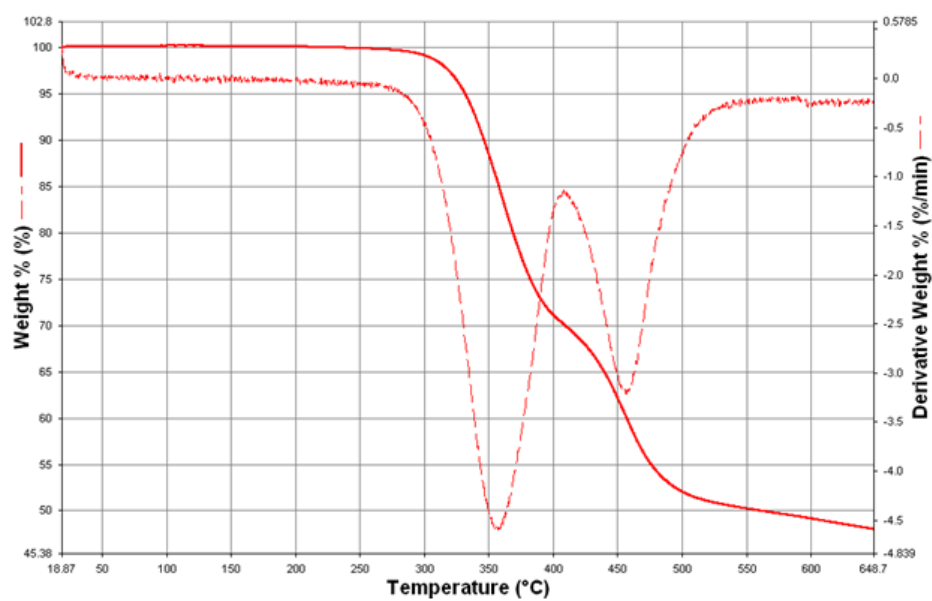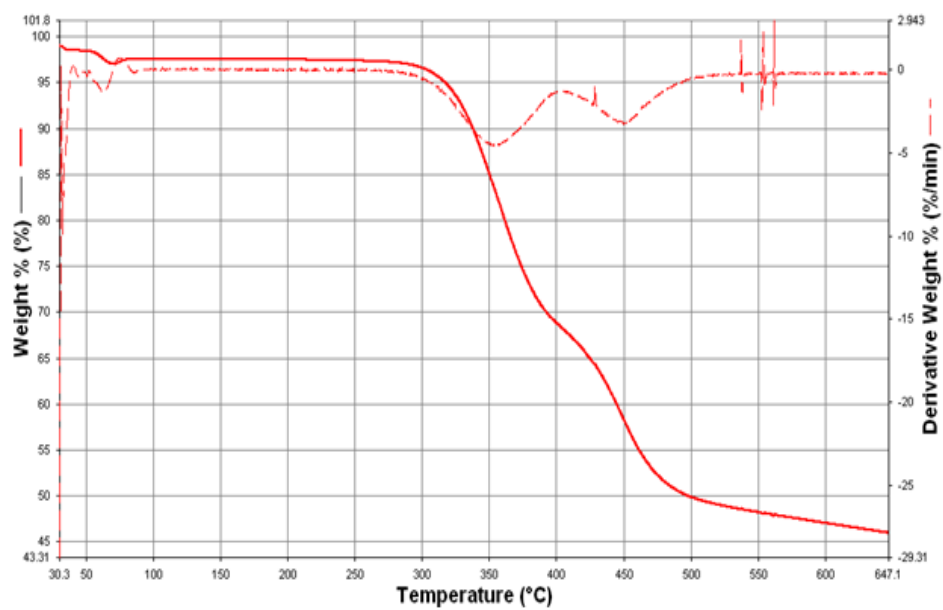
Figure 39. TGA study of **P1**

Figure 40. TGA study of **P2**

CHAPTER 6

CONCLUSION

In this study, two strong electron acceptor moieties; benzothiadiazole and benzotriazole were used on the same polymer backbone and two different random polymers were synthesized. Investigation of effects of electron-withdrawing fluorine atom on electrochemical and optoelectronic properties was achieved using nonfluorinated and fluorinated benzothiadiazoles. The purpose of having fluorine atom on polymer backbone was to decrease HOMO and LUMO energy levels, and to increase V_{oc} and PCE%. Following by electrochemical, spectroelectrochemical, kinetic and optical characterization, the polymers were used to construct bulk heterojunction organic solar cells.

According to electrochemical studies, the polymers were only p-dopable. Electron-withdrawing fluorine atom made **P2** more electron deficient. Thus, **P2** showed higher oxidation potential that of nonfluorinated **P2**. HOMO energy levels of the polymers were calculated from cyclic voltammograms. As expected **P2** had a deeper HOMO level since it contains fluorine atom in its backbone. In the light of optical studies, it was observed that polymers showed similar absorption spectra with different λ_{max}^{onset} values. From these data, optical band gaps of the **P1** and **P2** were determined as 1.78 eV and 1.72 eV, respectively. Since both polymers were not n-dopable, LUMO energy levels were calculated using optical band gaps. These calculations showed that adding fluorine atom to the polymer backbone decrease not only HOMO but also LUMO level. Reasonable HOMO and LUMO energy levels and optical band gap values revealed that polymers were proper for construction of organic solar cell.

Upon stepwise oxidation, spectroelectrochemistry data were recorded. With the information received, kinetic studies were performed. The highest optical contrast was observed in **P1** with 59 %. On the other hand, **P2** exhibited the fastest switching times and highest coloration efficiency because of efficient packing resulted from backbone fluorination.

In colorimetry studies, colors of both polymers in neutral states were dark blue and oxidized states were dark grey. These color change upon applied potential was resulted from electrochromic behavior of the polymers. The colors were reported in according to the CIE coordinates.

The polymers were used as the donor compartments in the bulk heterojunction organic solar cell where PCBM was the acceptor. Among them, the highest PCE was 4.13 % with DIO additive for **P1**. On the other hand, **P2** has 3.80 % PCE without any additive. It is expected that OSC device performance of these polymers might be enhanced by some structural modifications.

REFERENCES

(1)   World Energy Council. *World Energy Resources*; 2016.

(2)   REN21 Secretariat. *Renewables 2015 Global Status Report*; Paris, 2015.

(3)   Mohammad Bagher, A. *Int. J. Renew. Sustain. Energy* **2014**, *3* (3), 53.

(4)   Green, M. A.; Emery, K.; Hishikawa, Y.; Warta, W.; Dunlop, E.; Levi, D.; Baillie, A. *Prog. Photovolt Res. Appl.* **2017**, *25*, 10.

(5)   Glowacki, E. D.; Sariciftci, N. S. *Organic Solar Cells*; 2012.

(6)   Scharber, M. C.; Sariciftci, N. S. *Prog. Polym. Sci.* **2013**, *38* (12), 1929.

(7)   Uddin, M. A.; Chan, H. P.; Rahman, B. M. A. *Rev. Adv. Mater. Sci.* **2010**, *26* (2), 58.

(8)   Clarke, T. M.; Durrant, J. R. *Chem. Rev.* **2010**, *110* (11), 6736.

(9)   Winder, C.; Sariciftci, N. S. *J. Mater. Chem.* **2004**, *14* (7), 1078.

(10)   Günes, S.; Neugebauer, H.; Sariciftci, N. S. *Chem. Rev.* **2007**, *107* (4), 1328.

(11)   Krebs, F. C. *Sol. Energy Mater. Sol. Cells* **2009**, *93* (4), 394.

(12)   Brumbach, M.; Veneman, P. A.; Matrikar, F. S.; Schulmeyer, T.; Simmonds, A.; Xia, W.; Lee, P.; Armstrong, N. R. *Langmuir* **2007**, *23* (22), 11089.

(13)   Schlaf, R.; Murata, H.; Kafafi, Z. . *J. Electron Spectros. Relat. Phenomena* **2001**, *120* (3), 149.

(14)   Singh, A.; Garg, A. *RSC Adv.* **2015**, *5*, 78678.

(15)   Glowacki, E. D.; Marshall, K. L.; Tang, C. .; Sariciftci, N. S. *Appl. Phys. Lett.* **2011**, *99*, 3.

(16)   Oh, S. S.; Yeo, D. H.; Park, K. H.; Kim, H. B.; Ha, M. H.; Oh, H. J.; Park, M. W.; Park, J. S.; Park, D. W.; Jung, D. G.; Chae, H. Y.; Kim, H. S.; Boo, J. H.; Nam, E. Y. *Adv. Mater. Res.* **2012**, 1608.

(17)   Sun, S. S.; Sariciftci, N. S. *Organic Photovoltaics: Mechanisms, Materials, and Devices*; CRC Press: New York, 2005.

(18)   Menke, S. M.; Holmes, R. J. *Energy Environ. Sci.* **2014**, *7* (2), 499.

(19)   Vivek, K. A.; Agrawal, G. D. *Int. J. Res. Eng. Technol.* **2014**, *3* (9), 2319.

(20)   Nguyen, T.-Q.; Yee, R. Y.; Schwartz, B. J. *J. Photochem. Photobiol. A Chem.* **2001**, *144*, 21.

(21)   Facchetti, A. *Chem. Mater.* **2011**, *23* (3), 733.

(22)   Group, H. I. Cool Roofs https://heatisland.lbl.gov/coolscience/cool-roofs (accessed Jul 7, 2017).

(23)   Kim, J. Y.; Lee, K.; Coates, N. E.; Moses, D.; Nguyen, T.; Dante, M.; Heeger, A. J. *Science.* **2007** , 223.

(24)   Wallace, G. G.; Dastoor, P. C.; Officer, D. L.; Too, C. O. *Chem. Innov.* **2000**, *30* (4), 22.

(25)   Winder, C.; Matt, G.; Hummelen, J. C.; Janssen, R. A. J.; Sariciftci, N. S.; Brabec, C. J. *Thin Solid Films* **2002**, *403*.

(26)   Havinga, E. E.; Hoeve, W. ten; Wynberg, H. *Synth. Met.* **1993**, *55* (1), 299.

(27)   Hammed, W. A.; Yahya, R.; Bola, A. L.; Mahmud, H. N. M. E. *Energies* **2013**, *6* (11), 5847.

(28)   Huang, Y.; Kramer, E. J.; Heeger, A. J.; Bazan, G. C. *Chem. Rev.* **2014**, *114* (14), 7006.

(29) Beaupré, S.; Belletête, M.; Durocher, G.; Leclerc, M. *Macromol. Theory Simulations* **2011**, *20* (1), 18.

(30) Cheng, P.; Zhan, X. *Chem. Soc. Rev.* **2016**, *45* (9), 2544.

(31) Zhang, Z. G.; Wang, J. *J. Mater. Chem. View* **2012**, *22*, 4178.

(32) Pilgram, K.; Zupan, M.; Skiles, R. *J. Heterocycl. Chem.,* **1970**, *7*, 629.

(33) Mullekom, H. A. M. van; Vekemans, J. A. J. M.; Meijer, E. W. *Chem. Commun.* **1996**, 2163.

(34) Huang, Y.; Liu, F.; Guo, X.; Zhang, W.; Gu, Y.; Zhang, J.; Han, C. C.; Russell, T. P.; Hou, J. *Adv. Energy Mater.* **2013**, *3* (7), 930.

(35) Liu, C.; Wang, K.; Gong, X.; Heeger, A. J. *Chem. Soc. Rev.* **2015**, *45*.

(36) Hou, J.; Park, M.; Zhang, S.; Yao, Y.; Chen, L.; Li, J.; Yang, Y. *Macromol. 2008,* **2008**, *41*, 6012.

(37) Coffin, R. C.; Macneill, C. M.; Peterson, E. D.; Ward, J. W.; Owen, J. W.; Mclellan, C. A.; Smith, G. M.; Noftle, R. E.; Jurchescu, O. D.; Carroll, D. L. *J. Nanotechnol.* **2011**, *2011*, 3.

(38) Qu, B.; Yang, H.; Tian, D.; Liu, H.; Cong, Z.; Gao, C.; Chen, Z.; Xiao, L.; Gao, Z.; Wei, W.; Gong, Q. *Synth. Met.* **2012**, *162*, 2022.

(39) Zhang, Z.; Peng, B.; Liu, B.; Pan, C.; Li, Y.; He, Y. *Polym. Chem.* **2010**, *1*, 1443.

(40) Kim, J.; Un, H.; Eun, C.; Kang, I.; Lee, J.; Suk, W. *Sol. Energy Mater. Sol. Cells* **2013**, *108*, 115.

(41) Istanbulluoglu, C.; Göker, S.; Hizalan, G.; Hacioglu, S. O.; Udum, Y. A.; Yildiz, E. D.; Cirpan, A.; Toppare, L. *New J. Chem.* **2015**, *39*, 6625.

(42) Unay, H.; Unlu, N. A.; Hizalan, G.; Hacioglu, S. O.; Yildiz, D. E.; Toppare, L.; Cirpan, A. **2015**, 528.

(43)   Falzon, M.-F. F.; Wienk, M. M.; Janssen, R. a. J. *J. Phys. Chem. C* **2011**, *115* (7), 3178.

(44)   Karakus, M.; Apaydn, D. H.; Yldz, D. E.; Toppare, L.; Cirpan, A. *Polymer.* **2012**, *53* (6), 1198.

(45)   Kotowski, D.; Luzzati, S.; Bianchi, G.; Calabrese, A.; Pellegrino, A.; Po, R.; Schimperna, G.; Tacca, A. *J. Mater. Chem. A* **2013**, *1* (36), 10736.

(46)   Chen, H.; Hou, J.; Zhang, S.; Liang, Y.; Yang, G.; Yang, Y. *Nat. Photonics* **2009**, *3*, 649.

(47)   Liang, B. Y.; Xu, Z.; Xia, J.; Tsai, S.; Wu, Y.; Li, G.; Ray, C.; Yu, L. *Adv. Mater.* **2010**, *22*, 135.

(48)   Son, H. J.; Wang, W.; Xu, T.; Liang, Y.; Wu, Y.; Li, G.; Yu, L. *J. Am. Chem. Soc.* **2011**, *133*, 1885.

(49)   Zhou, H.; Yang, L.; Stuart, A. C.; Price, S. C.; Liu, S.; You, W. *Angew. Chem., Int. Ed.* **2011**, *50*, 2995.

(50)   Stuart, A. C.; Tumbleston, J. R.; Zhou, H.; Li, W.; Liu, S.; Ade, H. *J. Am. Chem. Soc.* **2013**, *135*, 1814.

(51)   Leclerc, N.; Chávez, P.; Ibraikulov, O. A.; Heiser, T.; Lévêque, P. *Polymers .* **2016**, *8* (11), 4.

(52)   Cevher, S. C.; Unlu, N. A.; Ozelcaglayan, A. C.; Apaydin, D. H.; Udum, Y. A.; Toppare, L.; Cirpan, A. *J. Polym. Sci.* **2013**, *51*, 1935.

(53)   Cho, N.; Song, K.; Lee, J. K.; Ko, J. *Chem. Eur. J.* **2012**, *18*, 11434.

(54)   Kim, J.; Yun, M. H.; Kim, G.; Lee, J.; Lee, S. M.; Ko, S.; Kim, Y.; Dutta, G. K.; Moon, M.; Park, S. Y.; Kim, D. S.; Kim, J. Y.; Yang, C. *ACS Appl. Mater. Interfaces* **2014**, *6*, 7525.

(55)   Xu, X.; Wu, Y.; Fang, J.; Li, Z.; Wang, Z.; Li, Y. *Chem. Eur. J.* **2014**, *20*, 13261.

(56)   Tregnago, G.; Steckler, T. T.; Fenwick, O.; Andersson, M. R.; Cacialli, F. *J. Mater. Chem. C* **2015**, *3*, 2793.

(57)   Unlu, N. A.; Deniz, T. K.; Sendur, M.; Cirpan, A. *Macromol. Chem. Phys.* **2012**, *213* (18), 1885.

(58)   Ford, A.; Roberts, A. *Westminster Univ. London* **1998**, *1998*, 31.

(59)   Fei, Z.; Shahid, M.; Yaacobi-Gross, N.; Rossbauer, S.; Zhong, H.; Watkins, S. E.; Anthopoulos, T. D.; Heeney, M. *Chem. Commun.* **2012**, *48* (90), 11130.

(60)   Liu, P.; Zhang, K.; Liu, F.; Jin, Y.; Liu, S.; Russell, T. P.; Yip, H.-L.; Huang, F.; Cao, Y. *Chem. Mater.* **2014**, *26*, 3009.

(61)   Yuan, M.; Yang, P.; Durban, M. M.; Luscombe, C. K. *Macromolecules* **2012**, *45* (15), 5934.

(62)   Yang, P.; Yuan, M.; Zeigler, D. F.; Watkins, S. E.; Lee, J. A.; Luscombe, C. K. *J. Mater. Chem. C* **2014**, *2* (17), 3278.

(63)   Price, S. C.; Stuart, A. C.; Yang, L.; Zhou, H.; You, W. *J. Am. Chem. Soc.* **2011**, *133* (12), 4625.

(64)   Akbayrak, M.; Önal, A. M. *Polym. Chem.* **2016**, *7* (39), 6110.

(65)   Neo, W. T.; Ong, K. H.; Lin, T. T.; Chua, S.-J.; Xu, J. *J. Mater. Chem. C* **2015**, *3* (21), 5589.

(66)   Li, Z.; Lu, J.; Tse, S.-C.; Zhou, J.; Du, X.; Tao, Y.; Ding, J. *J. Mater. Chem.* **2011**, *21* (9), 3226.

(67)   Bronstein, H.; Frost, J. M.; Hadipour, A.; Kim, Y.; Nielsen, C. B.; Ashraf, R. S.; Rand, B. P.; Watkins, S.; McCulloch, I. *Chem. Mater.* **2013**, *25*, 277.
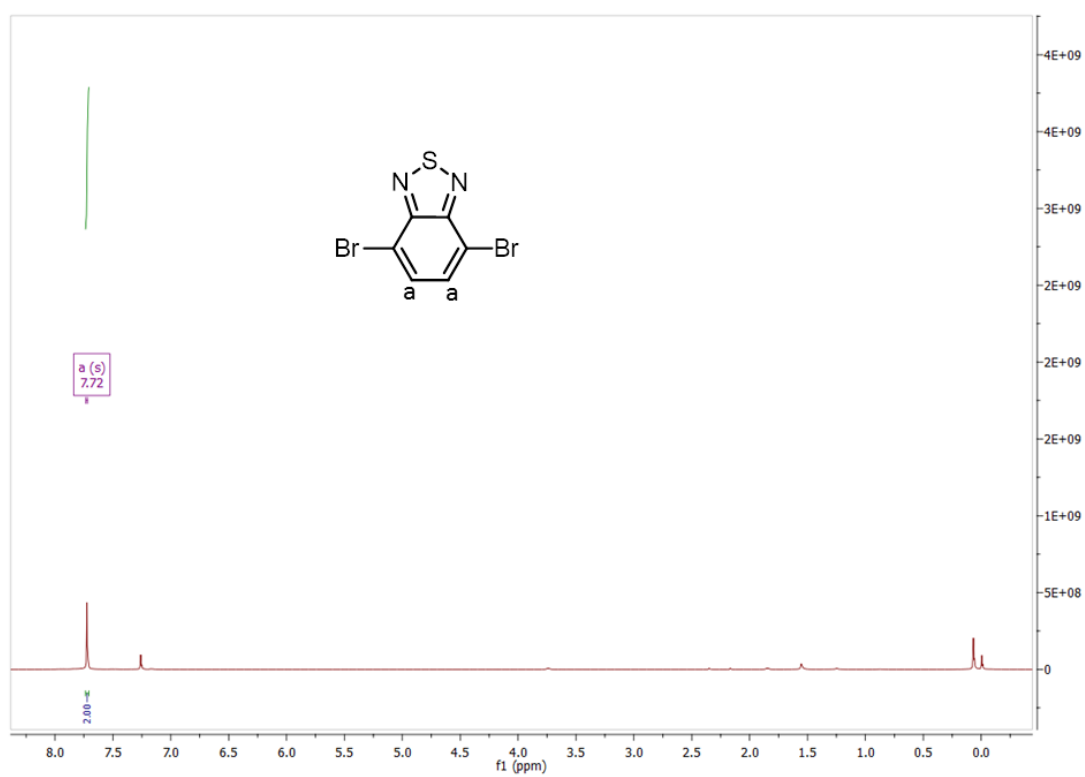
NMR DATA

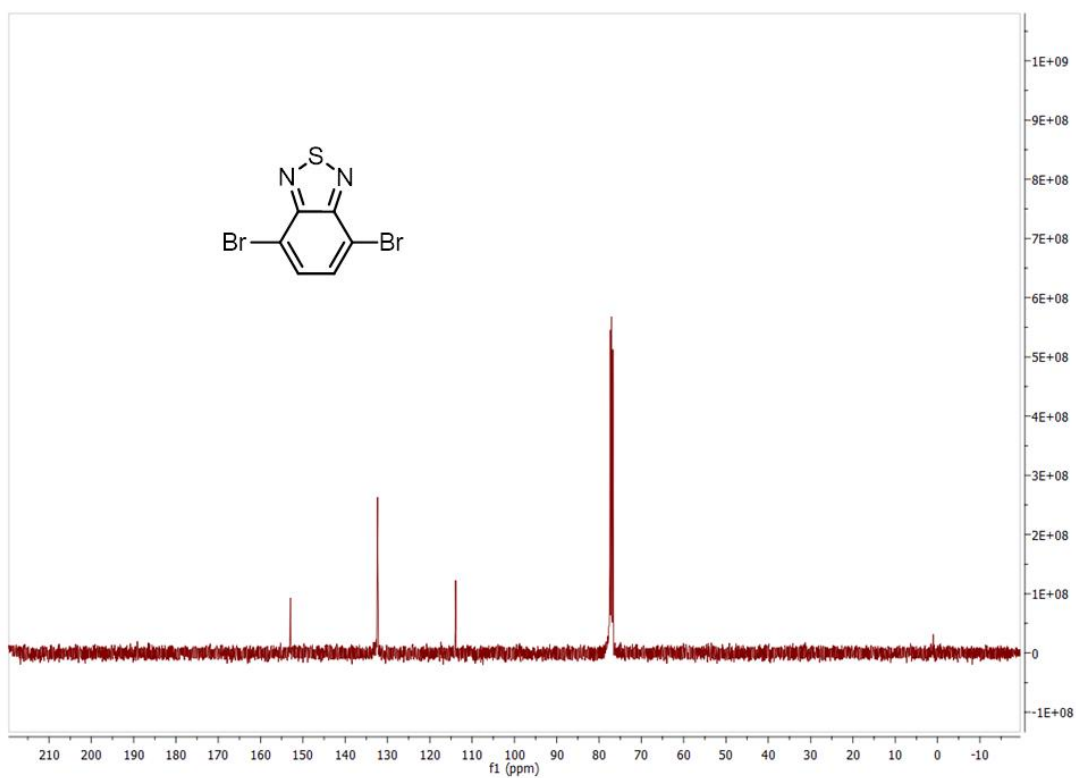**Figure A. 1.** ^{1}H NMR of 4,7-dibromo-2,1,3-benzothiadiazole

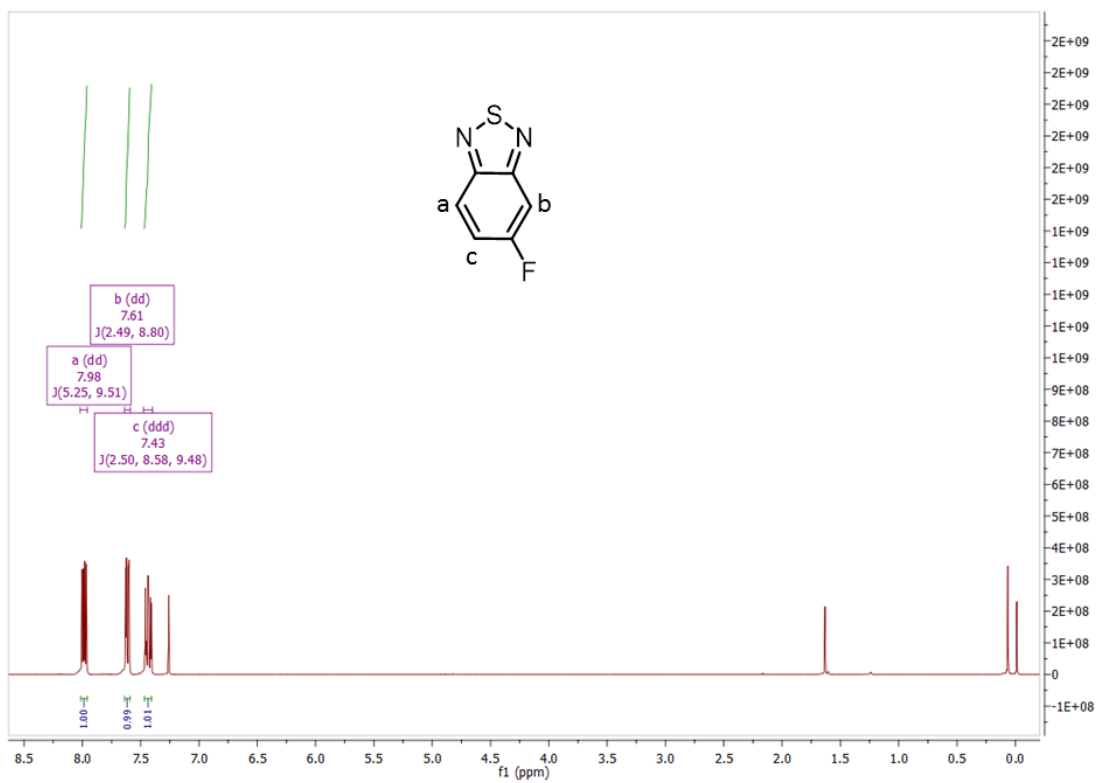**Figure A. 2.** ^{13}C NMR of 4,7-dibromo-2,1,3-benzothiadiazole

Figure A. 3. ^{1}H NMR of 5-fluoro-2,1,3-benzothiadiazole
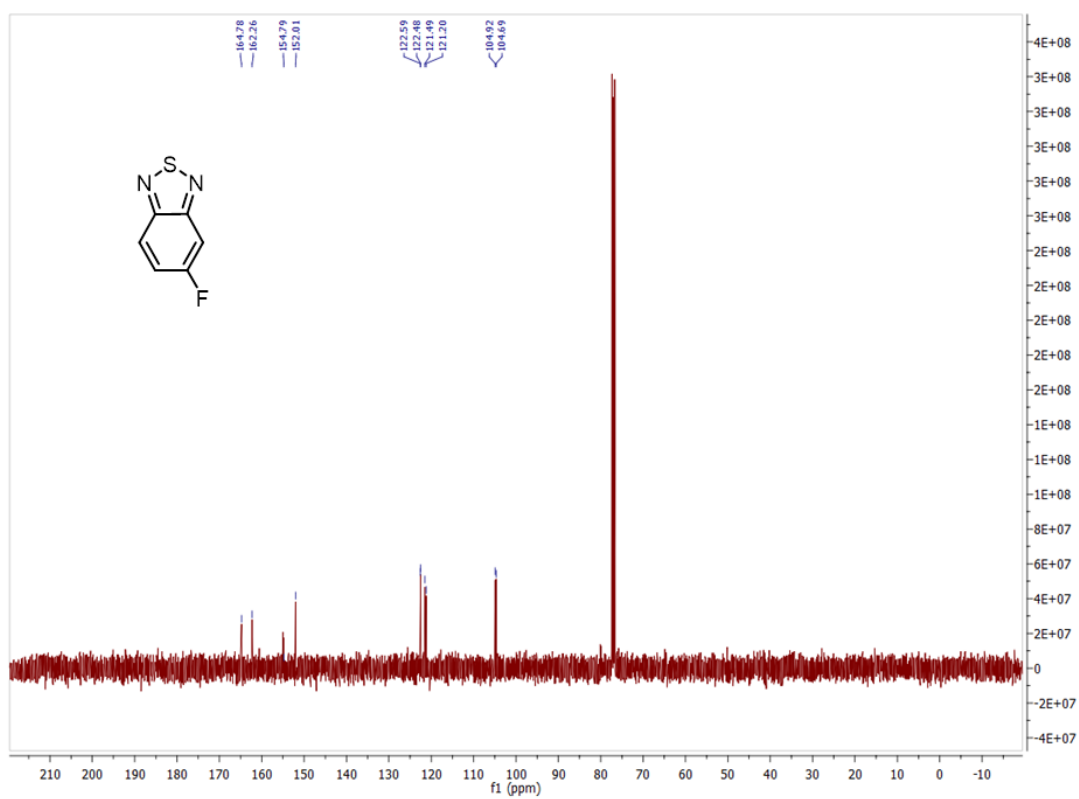
Figure A. 4. ^{13}C NMR of 5-fluoro-2,1,3-benzothiadiazole
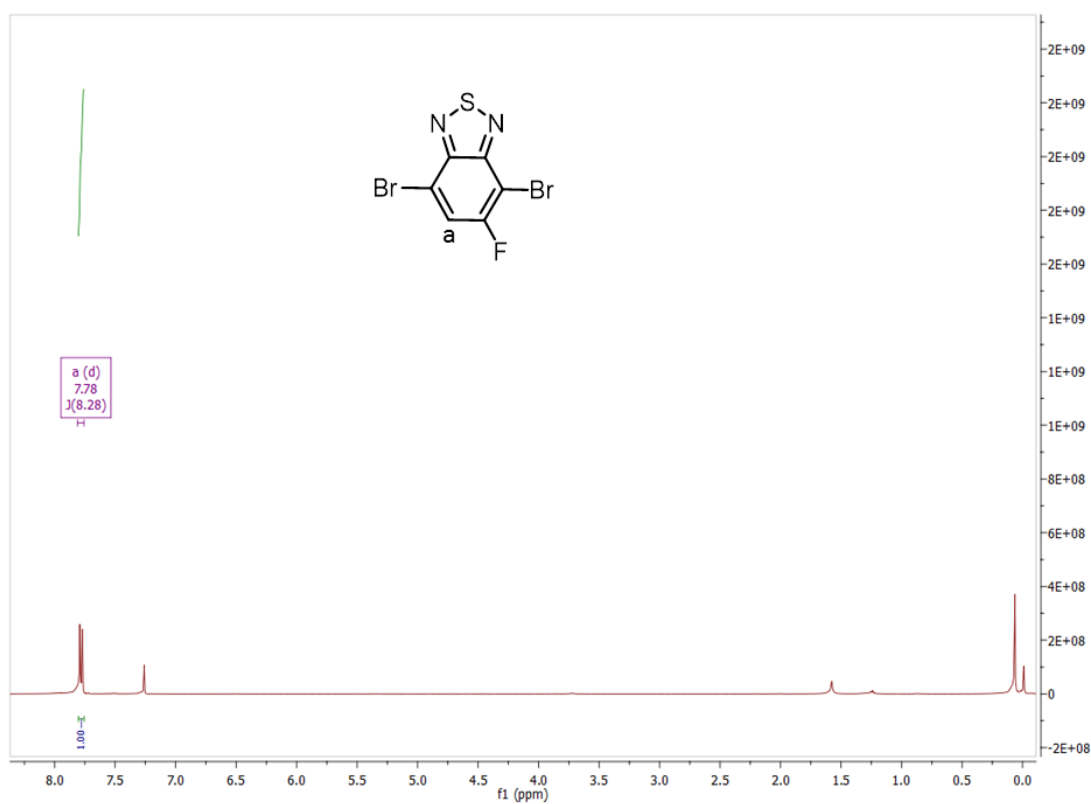
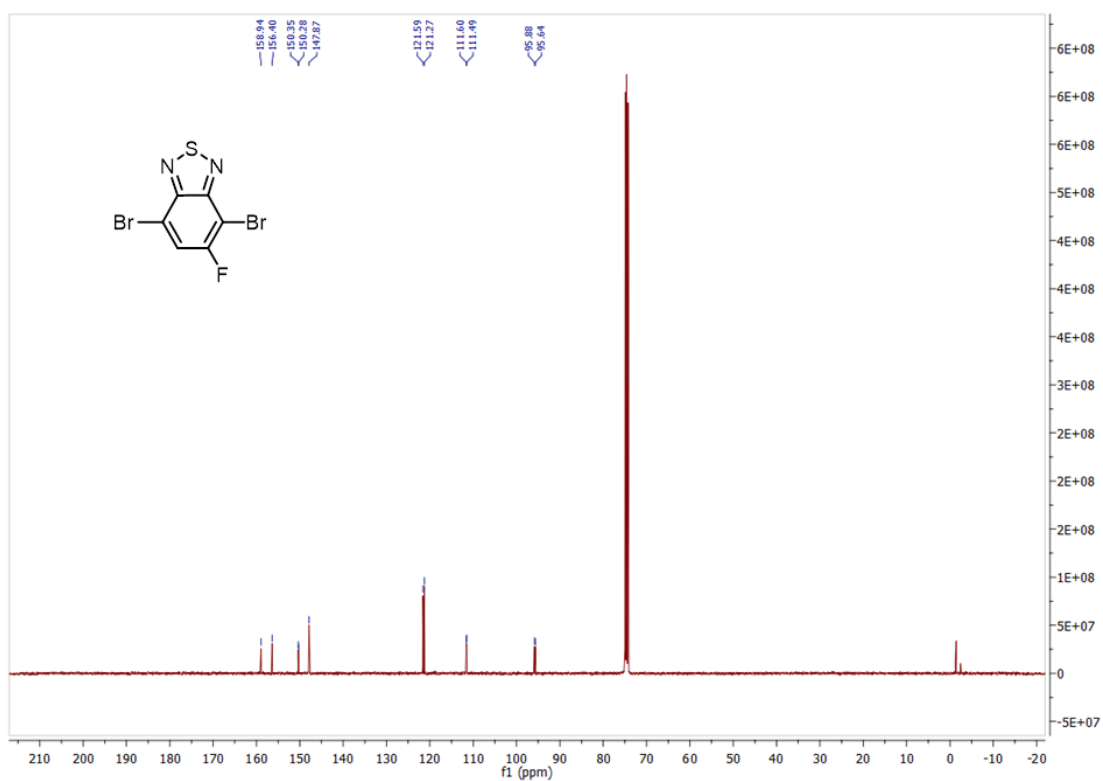**Figure A. 5.** ^{1}H NMR of 4,7-dibromo-5-fluoro-2,1,3-benzothiadiazole

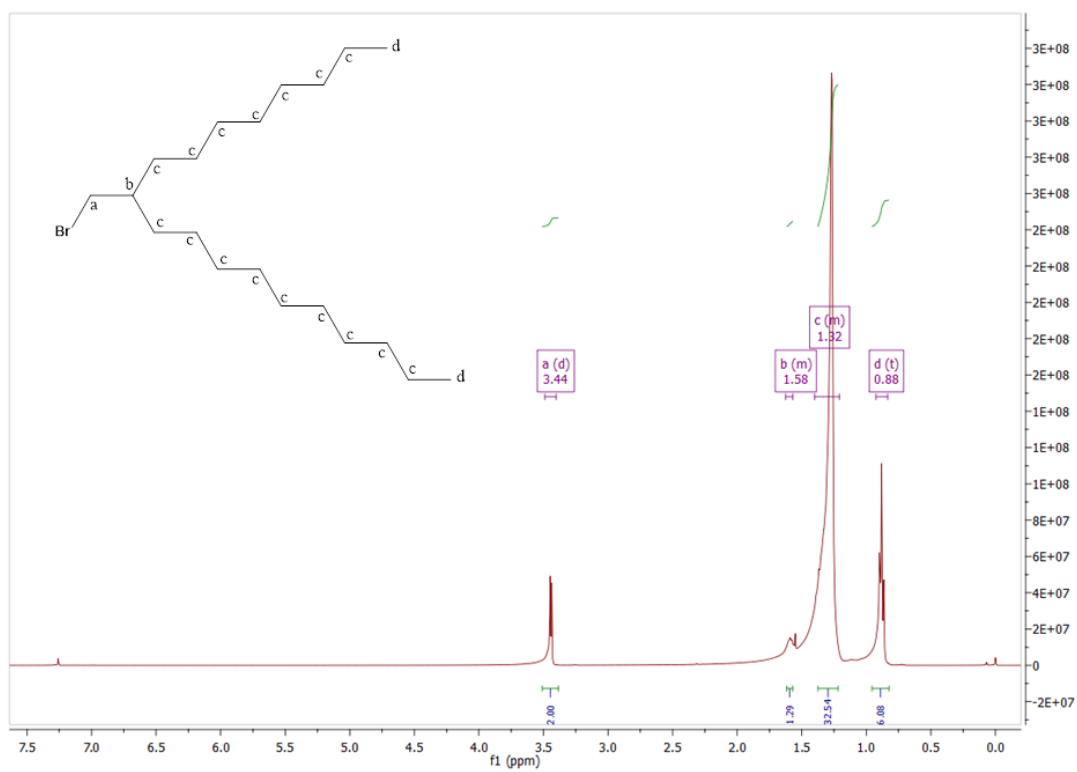**Figure A. 6.** ^{13}C NMR of 4,7-dibromo-5-fluoro-2,1,3-benzothiadiazole
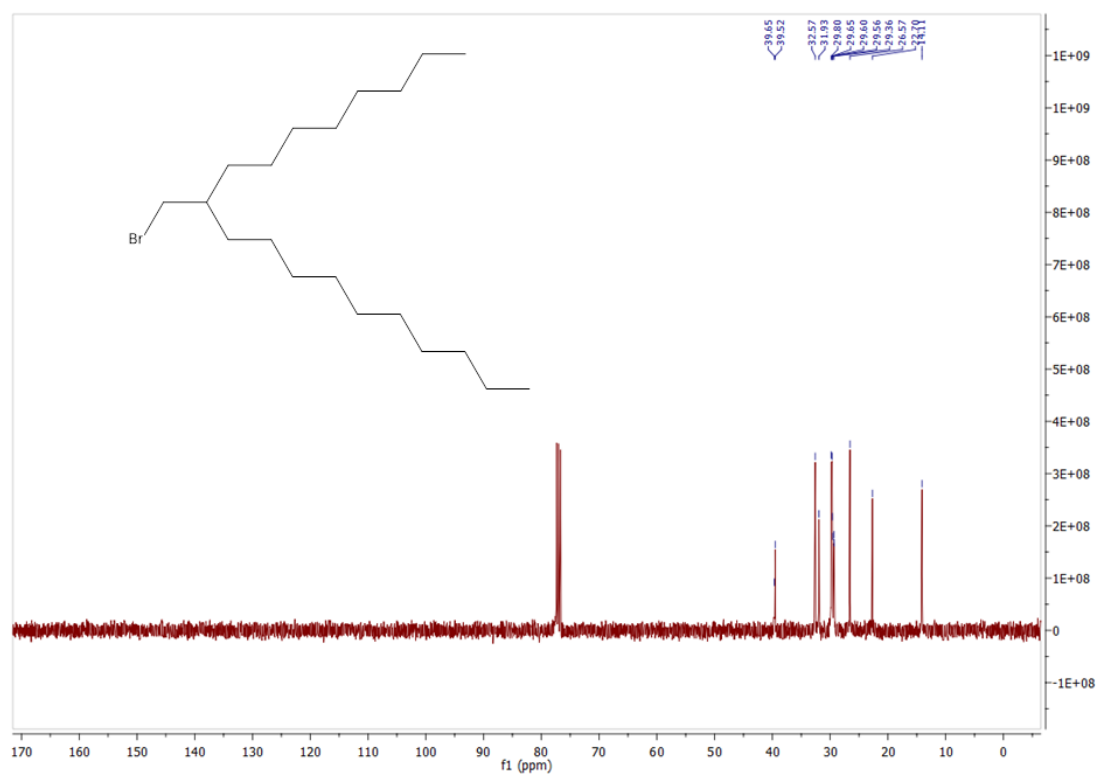
Figure A. 7. ^{1}H NMR of 9-(bromomethyl) nonadecane

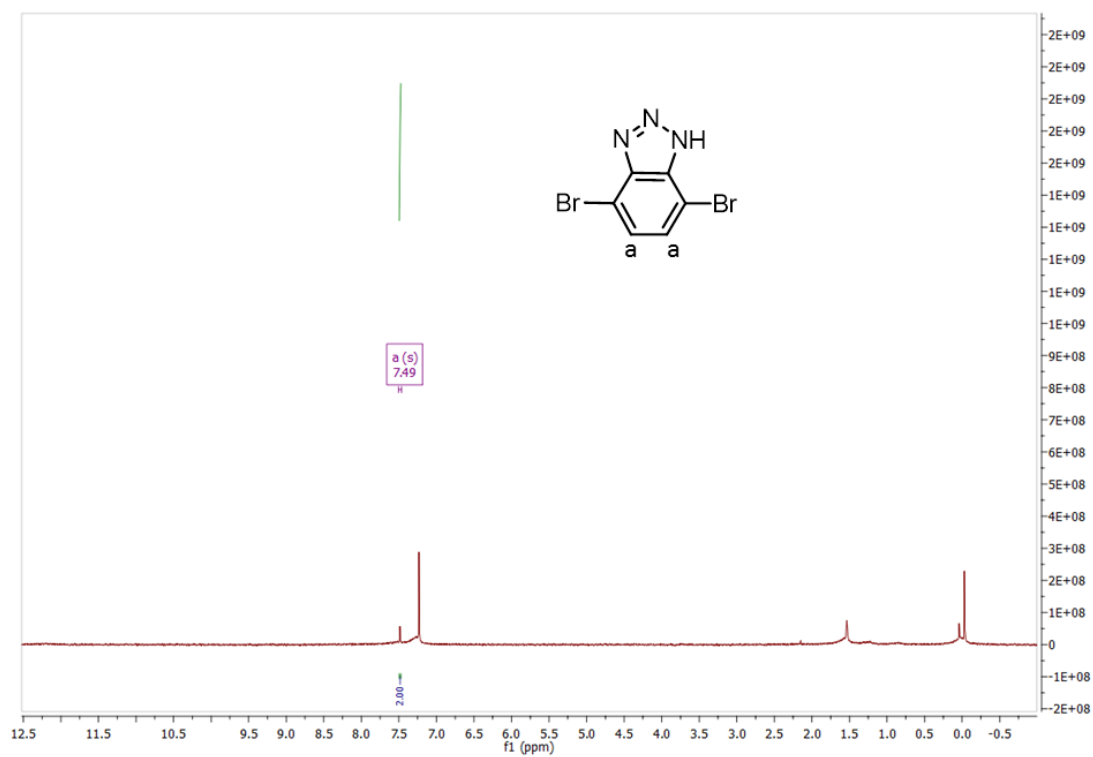**Figure A. 8.** ^{13}C NMR of 9-(bromomethyl) nonadecane

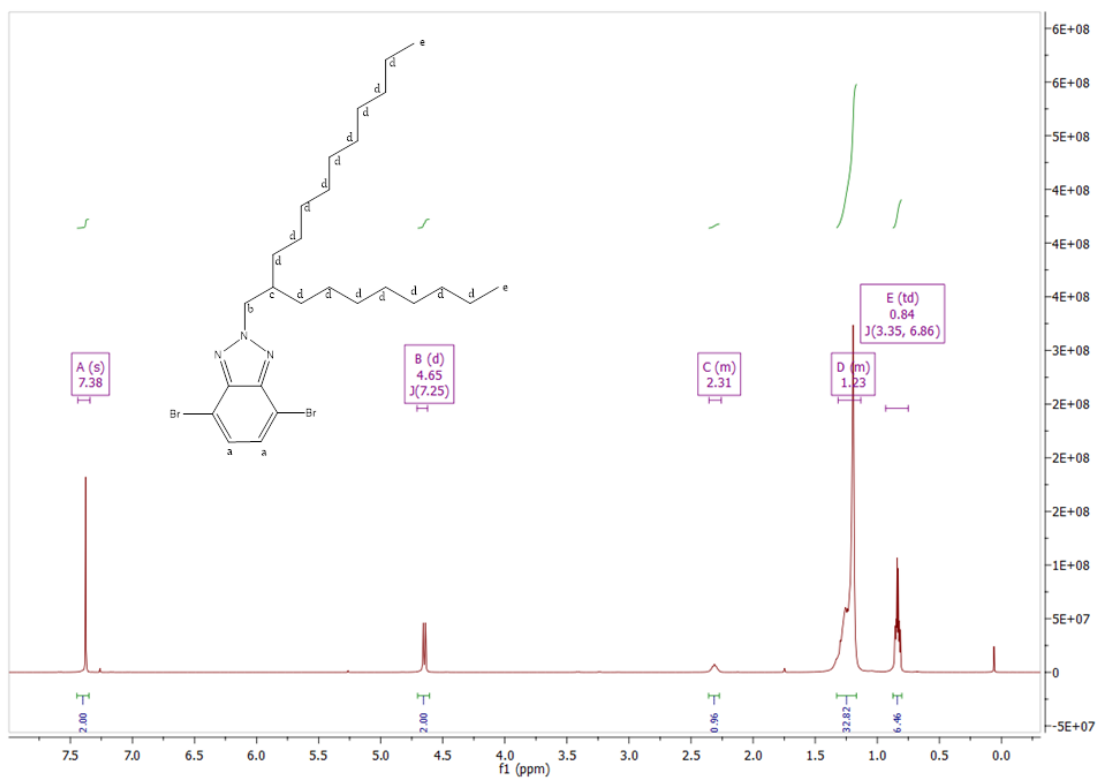**Figure A. 9.** ^{1}H NMR of 4,7-dibromo-1H-benzotriazole

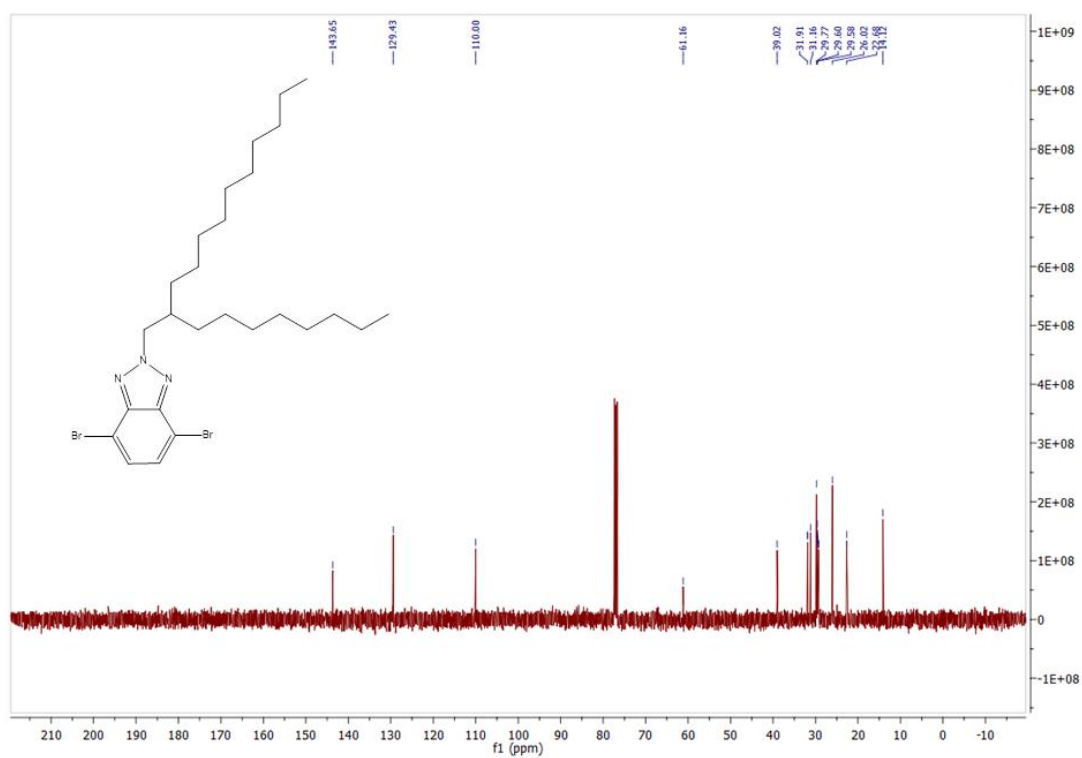**Figure A. 10.** ^{1}H NMR of 4,7-dibromo-2-(2-octyldodecyl)-benzotriazole

Figure A. 11. ^{13}C NMR of 4,7-dibromo-2-(2-octyldodecyl)-benzotriazole